Article:
Wang, D, Samsulrizal, N, Yan, C et al. (2019) Characterisation of CRISPR mutants targeting genes modulating pectin degradation in ripening tomato. Plant Physiology, 179 (2). pp. 544-557. ISSN: 0032-0889

https://doi.org/10.1104/pp.18.01187

Short Title: Tomato cell wall mutants and ripening

Characterisation of CRISPR mutants targeting genes modulating pectin degradation in ripening tomato.

Duoduo Wang [a], Nurul H. Samsulrizal [b], Cheng Yan [C], Natalie S. Allcock [d], Jim Craigon[a], Barbara Blanco-Ulate[e], Isabel Ortega-Salazar,[e] Susan E. Marcus[f], Hassan Moeiniyan Bagheri[a], Laura Perez-Fons[g], Paul D. Fraser[g], Timothy Foster [a], Rupert Fray [a], J. Paul Knox [f] and Graham B. Seymour [a] *

[a] School of Biosciences, University of Nottingham, Sutton Bonington, Loughborough, LEICS. LE12 5RD, UK.

[b] Department of Plant Science, Kulliyyah of Science, International Islamic University Malaysia.

[c] Institution of Vegetable Research, Shanxi Academy of Agricultural Sciences, 79 Longcheng Street, Xiaodian District, Taiyuan City, Shanxi Province, China 030031.

[d] Electron Microscopy Facility, Centre for Core Biotechnology Services, University of Leicester, University Road, Leicester, LE1 7RH, UK

[e] Plant Sciences Department, University of California, Davis, California, 95616, USA.

[f] Centre for Plant Sciences, Faculty of Biological Sciences, University of Leeds, Leeds LS2 9JT, UK

[g] School of Biological Sciences, Plant Molecular Sciences, Centre for Systems and Synthetic Biology, Royal Holloway, University of London, Egham, Surrey, TW20 0EX, UK

ORCID IDs: 0000-0001-8365-4947 (G.B.S) 0000-0002-9231-6891 (J.P.K)

*Corresponding author: graham.seymour@nottingham.ac.uk (Graham B. Seymour)

One-sentence summary: Comparative analysis of CRISPR mutations in tomato cell wall genes indicated only pectate lyase had a major impact on fruit softening, but other enzymes played an important role in coordinating controlled cell wall disassembly.

Key words: Tomato, Ripening, Softening, CRISPR, Polygalacturonase, Pectate Lyase, Galactanase, Pectin

Author Contributions:

G.B.S and D.D.W conceived the original research plans. D.D.W performed the majority of the experiments and analysed the data. D.D.W and G.B.S wrote the manuscript. N.H.S and C.Y were involved in generating CRISPR lines. PF and LP undertook the carotenoid analysis and were involved in writing the paper. SM and HB performed the cell wall analysis. N.S.A performed electron microscopy. J.C provided assistance with statistical analysis. B.B-U and I.B.O.S contributed Supplementary Fig. 5 and to writing the paper. T.F., R.F., J.P.K were involved with writing the paper. All authors were involved in reviewing and editing the manuscript.

Abstract

Tomato is a globally important crop with an economic value of $10s bn, and relevant in supplying essential vitamins, minerals and phytochemicals in the human diet. Shelf life is a key quality trait related to alterations in cuticle properties and remodelling of the fruit cell walls. Studies with transgenic tomato plants undertaken over the last 20 years have indicated that a range of pectin degrading enzymes are involved in cell wall remodelling. These studies usually involved silencing of only a single gene and it has proved difficult to compare the effects of silencing these genes across the different experimental systems. Here we report the generation of CRISPR-based mutants in the ripening-related genes encoding the pectin degrading enzymes pectate lyase (PL), polygalacturonase 2a (PG2a) and β-galactanase (TBG4). Comparison of the physiochemical properties of the fruits from a range of *PL*, *PG2a* and *TBG4* CRISPR lines demonstrated that only mutations in *PL* resulted in firmer fruits, although mutations in *PG2a* and *TBG4* influenced fruit colour and weight. Pectin localisation, distribution and solubility in the pericarp cells of the CRISPR mutant fruits was investigated using the monoclonal antibody probes LM19 to de-esterified homogalacturonan (HG), INRA-RU1 to rhamnogalacturonan I, LM5 to β1-4-galactan and LM6 to arabinan epitopes respectively. The data indicate that PL, PG2a and TBG4 act on separate cell wall domains and the importance of cellulose microfibril associated pectin is reflected in its increased occurrence in the different mutant lines.

Introduction

Many fleshy fruits undergo pronounced softening during the ripening process. Softening is important for flavour development and overall palatability, but also impacts fruit storage, transportability and shelf life (Klee and Giovannoni, 2011). High quality produce with a long shelf life is essential for the modern supply chain. Current methods for slowing the softening process in tomato involve the use of hybrids containing non-ripening mutations that in the heterozygous form can enhance postharvest life, but these non-ripening genes can also compromise other aspects of ripening including flavour and colour development (Kitagawa et al., 2005). A better strategy would be to target just the softening process alone.

A substantial amount of work has been undertaken to investigate the genetic and molecular basis of fruit softening. Fruit texture is determined by numerous factors including cell wall structure (Seymour et al, 2013), cellular turgor (Saladié et al., 2007), hydroxyl radical (·OH) attack (Airianah et al., 2016) and cuticle properties (Yeats and Rose, 2013). Remodelling of the cell wall is thought to be a predominant mechanism for inducing softening involving changes in the complex networks of microfibril and matrix polysaccharides including cellulose, hemicelluloses, pectins, and structural proteins (Keegstra, 2010). The primary cell walls and middle lamellae (ML) of fruits are normally rich in pectin and these pectic polysaccharides have long been known to undergo degradation during the ripening process (Brummell, 2006).

Pectins are the most structurally complex plant cell wall polysaccharides, and three major classes of these polymers have been identified: homogalacturonan (HG), rhamnogalacturonan-I (RG-I) and rhamnogalacturonan-II (RG-II) (Atmodjo et al., 2013). Evidence indicates that during ripening these high molecular weight polymers are being released from the wall matrix likely through breaking of covalent linkages (Brummell, 2006). The pectic polymers also undergo a loss of neutral sugar side chains (associated with RG-I) and methyl ester groups from HG (Wang et al., 2018). In tomato, strawberry and many other fruits these changes are brought about by suites of cell wall degrading enzymes (see Table 1 in Wang et al., 2018), with varying cocktails of activities in different species.

Over the past 40 years a wide range of enzymes have been investigated to determine which activities are involved in regulating fruit softening. Work on tomato has included the generation of transgenic plants to silence the activity of genes encoding polygalacturonase (PG),

pectinesterase (PE), galactanase (TBG), xyloglucan endo-transglycosylase (XTH) and expansin (Smith et al., 1988; Sheehy et al., 1988; Tieman and Handa, 1994; Brummell et al., 1999; Smith et al., 2002; Cantu et al, 2008). These experiments have yielded only modest changes in texture of the transgenic fruits. However, in strawberry, a model for non-climacteric fruits, suppression of either pectate lyase (*PL*) or *PG* resulted in much firmer fruit (Jiménez-Bermúdez et al., 2002; Quesada et al., 2009). More recently silencing of *PL* in tomato has been shown to inhibit fruit softening (Uluisik et al., 2016). Pectin degradation has therefore been demonstrated to be a major determinate of softening in fleshy fruits.

New insights into the structure of primary cell walls are providing a way to further characterise the role of pectin degradation in fruit softening. Until recently pectin was thought to contribute to wall mechanics relatively independently of other cell wall polymers such as cellulose and xyloglucan. The pectic polysaccharides were considered to influence cell wall properties mainly through their ability to form so-called 'egg box' structures, in which divalent calcium ions cross-linked chains of de-esterified HG, leading to strengthening of the gel matrix independent of any cellulose-pectin interactions (Carpita and Gibeaut, 1993). In this "tethered network" model, cellulose microfibrils are coated and interlocked by xyloglucan, or other hemicellulose polymers, forming the load-bearing network. However, the validity of this conventional cell wall model has been challenged by a series of recent discoveries. It has been proposed that pectin may directly contribute to the crosslinking of cellulose microfibrils in the cell wall, potentially to a greater extent than xyloglucan, the classical crosslinking hemicellulose (Wang and Hong, 2016). Additionally, some subsets of xyloglucan and pectin can be covalently linked together (Thompson and Fry, 2000; Popper and Fry, 2005; Popper and Fry, 2008; Cornuault et al., 2018) and new structural features of pectic supramolecules have been recognised using atomic force microscopy (Round et al., 2010). They include branches on the main galactosyluronic acid backbone of the pectic polysaccharides. These novel observations may explain why pectin degradation can modulate fruit texture.

For this study, we leveraged available DNA editing technologies (Wang et al., 2014) to generate loss of function mutants in specific cell wall structural enzymes and, therefore, provide an opportunity to revisit their functions in the context of a new understanding of the structure of plant cell walls. We generated mutations in genes encoding the tomato pectin degrading enzymes PL, PG2a and TBG4 and analysed their effects on fruit softening and pectin localisation in the ripe fruit pericarp. We report that, in our comparative study, only the

silencing of *PL* had any significant impact on tomato softening, and that PL is necessary for: (i) changes in the pectin domains that lead to loss of de-esterified HG from tricellular junctions, and (ii) degradation of HG and RG-I by PG2a and TBG4. The presence of all three enzyme activities are needed, however, to allow normal ripening-related changes in pericarp cell-to-cell adhesion and solubilisation of pectin from association with cellulose microfibrils.

RESULTS

CRISPR/Cas9-induced homozygous lines were generated to silence *PECTATE LYASE* (*PL*), *POLYGALACTURONASE* (*PG2a*), and *β-GALACTANASE* (*TBG4*).

Single guide RNAs were designed to create individual mutations in the coding sequences of *PL, PG2a* and *TBG4* (Table S1). Specific sites were selected to avoid off-target mutagenesis using the tomato genome sequence v2.5 (https://solgenomics.net/). The sgRNAs were expressed under the control of the plant RNA polymerase III AtU6 promoter (Nekrasov et al., 2013). A total of 12, 10, and 7 transgenic plants were generated for *PL*, *PG2a,* and *TBG4*, respectively. Two homozygous lines were studied in detail for *PL* and *TBG4* respectively and three for *PG2a* (Figure 1). All were fully characterised in the T_1 generation. In addition, a transgene free T_1 line which had come through tissue culture, was used as the azygous wild type control. Analysis indicated that mutations in the CRISPR lines generated Premature Translation Termination Codons (PTC) in the mRNAs for the target genes. These resulted in nonsense mutations and truncated, incomplete, and non-functional protein products in the mutants (see Figure S1-S3).

PG2a, PL and *TBG4* gene expression and enzyme activity in the CRISPR lines

Expression of the *PL, PG2a*, and *TBG4* target genes was determined by quantitative RT-PCR(qPCR) using pericarp tissues of red ripe (Breaker+7) fruit. Transcripts of all the three genes were reduced in CRISPR mutants compared with azygous lines. A significant ($P<0.001$) difference in relative gene expression was detected (Figure S4) in the *PG2a* lines. All CRISPR lines would be expected to generate non-functional proteins (Figure S1-S3).

PL activity was estimated based on its β-eliminative reaction with cell wall-bound pectin.

The basis of the assay was an increase in absorbance at 232 nm of the clarified reaction mixture due to the release of 4,5-unsaturated products from cell wall preparations as a result of PL activity. This follows the method described by Collmer et al. (1988). Acetone insoluble preparations were used because we found that the enzyme could not be purified away from the cell wall material without complete loss of activity. PL activity in the CRISPR lines was significantly ($P<0.001$) reduced in comparison with the azygous controls Figure 2A. There was residual PL activity in the CRISPR lines and this likely resulted from other PL genes that are weakly expressed during ripening, such as *Solyc05g055510* and *Solyc02g093580* (Figure S5). The reduction of PL activity in the CRISPR knockout lines was consistent with that reported from the RNAi study published recently by Uluisik et al, (2016). PG2a enzyme activity was significantly ($P <0.001$) reduced in all the three independent CRISPR lines when compared with the azygous control at the red ripe (B+7) stage (Figure 2B). Residual PG activity was detected in these lines and this must arise from the products of other PG-like genes known to be expressed at low levels in ripening tomato (The Tomato Genome Consortium, 2012). Measurement of TBG4 activity was undertaken using a potato β-1-4-galactan-rich substrate. A significant ($P<0.001$) reduction in enzyme activity was apparent in the *TBG4* CRISPR lines (Figure 2C). Measurements of total β-galactosidase (Figure S6) failed to show a large reduction in the CRISPR lines, but this would be expected as most of the β-galactosidase activity in tomato pericarp is associated with other non-cell wall based isoforms (Pressey, 1983).

Effects of CRISPR mutations on ripening

Fruits from the *PL* CRISPR lines had significantly ($P<0.05$) firmer outer and inner pericarp tissues compared to the control, but fruits from the CRISPR edited *PG2a* and *TBG4* lines showed a similar degree of softening to the azygous controls (Figure 3 A and B). Pericarp colour at red ripe B+7 stage was similar in the *PL* and azygous controls. However, a significant ($P<0.05$) decrease in colour index was detected in both *PG2a* and *TBG4* lines (Figure 4A). Analysis of pericarp carotenoids indicated significantly ($P<0.05$) enhanced β-carotene and reduced *cis*-phytoene in the *TBG4* and *PG2a* lines. There was also a trend toward reduced lycopene levels in these lines although this was not significant (Figure S7). Such a profile suggests that ripening related carotenoid formation could have been affected indirectly in these CRISPR mutants. Fruit weight varied among mutant lines. The *TBG4*, *PG1* and *PG34* CRISPR lines had significantly ($P<0.05$) higher fruit weights than the azygous control fruit at the same stage of ripeness (Figure 4B). Measurement of the fresh weight to dry weight ratio (Table S2) indicated that the variation among the means was not significant ($P=0.111$). There were no

significant (P>0.05) differences between any of the CRISPR lines and the azygous control in soluble solids content (% Brix) of the fruit at the red ripe B+7 stage (Figure 4C).

Preliminary assessment of juice viscosity of the CRISPR lines was performed using RheolabQC rheometer. Juice viscosity was significantly (P<0.05) higher in *PL* and *PG2a* lines compared with the azygous control, with an effect on paste viscosity in one of the *TBG4* lines (Figure 5). Inhibiting PL and PG activity will permit the structural integrity of pectin polymers to be retained and therefore this would be predicted to have a positive influence on juice viscosity. Investigating the full impact of the CRISPR mutations on tomato processing traits is outside the scope of the present investigation and is now part of a further study.

Immunocytochemistry of cell wall de-esterified HG and β-1-4-galactan in CRISPR mutants

For the immunocytochemistry experiments, a single representative allele from each mutant class was selected and fruit were harvested at the orange ripe B+4 stage. This stage was chosen rather than red ripe B+7 because the activity of each of these cell wall enzymes has previously been shown to be at a maximum post breaker, but prior to the fully ripe stage (Della Penna et al., 1987; Smith and Gross, 2000; Uluisik et al., 2016; Yang et al., 2017). Also, preliminary experiments indicated that better fixation and localisation of pectin was achieved prior to fruit becoming fully ripe. All immunocytochemistry experiments were performed using multiple sections taken from embedded pericarp tissue from three biological replicates. The pericarp tissue from each line was fixed, embedded in resin and thin sections were cut and probed with the monoclonal antibodies LM19 and LM5. LM19 recognises unesterified HG (Verhertbruggen et al., 2009), LM5 recognises a linear tetrasaccharide at the non-reducing end of (1-4)-β-D-galactan that occurs as a sidechain of RG-I (Jones et al., 1997; Anderson et al., 2016).

Initially, thin sections from each of the lines were labelled with Calcofluor-white which binds strongly to cellulose (Figure S8). This showed that there were no major differences in cell size or patterning between the tomato lines. Under the transmission electron microscope cell walls of the various lines looked similar (Figure 6), although electron dense material was more often present in the tricellular junctions of the *PL* and *PG* CRISPR lines. Furthermore the intercellular spaces in the *TBG4* CRISPR fruits were often larger than in other lines,

particularly in the inner regions of the pericarp, indicating some loss of cell-to-cell adhesion at these points (Figure 6).

Probing the pericarp sections with LM19 indicated a higher epitope signal intensity in the pericarp *PL*, *PG2a*, and *TBG4* CRISPR lines than that of the azygous control (Figure 7). In the control, there was some labelling of the cell walls but the epitope was often absent from the cell junctions and ML regions (Figure 7). Higher levels of labelling with LM19 were apparent in all CRISPR lines. Analysis of the micrographs using Image J (Table S3) indicated that the *PG2a* CRISPR lines had the highest mean intensity of label, while azygous controls had the lowest. The intensity of labelling of the sections from the *TBG4* and *PL* CRISPR lines were similar, but higher than the control. There were significant ($P<0.05$) differences between the labelling intensity in the *PL* and *PG2a* CRISPR lines when compared against the azygous control (Table S3).

In sections of the *PL* CRISPR lines, the LM19 epitope was particularly abundant in cell walls at the tricellular junctions (Figure 7), a distinctive feature of the *PG2a* CRISPR line was the presence of LM19 labelling in the intercellular spaces at some of the tricellular junctions (the point between adherent and separated cell walls). An additional feature of the *PG2a* line was a discontinuous detection of the LM19 epitope in the adhered cell walls. In the *TBG4* CRISPR fruit pericarp, the LM19 epitope occurred evenly in cell walls and was often present in corners of cell wall junctions and partially present in the ML, but absent from the intercellular spaces (Figure 7).

The monoclonal antibody LM5 was used to detect β-1,4-galactan sidechains of RG-I. Low levels of labelling for LM5 were apparent in the azygous control with some labelling in the primary walls, but generally the signal was absent from the ML region. A similar pattern of labelling with LM5 to the controls was apparent in the *PG2a* line (Figure 7). Both the *PL* and *TBG4* CRISPR mutants showed much higher levels of LM5 labelling (Figure 7, Table S3). In the *PL* mutant the outer cell walls of epidermal cells were strongly labelled but the sub-epidermal cells reacted weakly with LM5, which was in contrast to *TBG4* CRISPR mutant where sub-epidermal cells were strongly labelled (Figure 7). LM5 labelling was evident in the region of the cell wall lining the intercellular spaces especially in the *PL* and *TBG4* lines. In both the *PL* and *TBG4* lines, LM5 binding was generally absent from the intercellular spaces and the tricellular cell junctions.

Extraction and characterisation of cell wall pectin fractions using pectin antibody probes

Cell wall material was prepared from the pericarp of Breaker+7 fruit of representative wild type, *PL*, *PG2a* and *TBG4* lines. Preparations of three biological replicates were then extracted sequentially with water, the calcium chelator cyclohexane diamine tetraacetic acid (CDTA) and 4 M KOH and then the residue treated with cellulase. The clarified extracts were then probed with a range of monoclonal antibodies to determine the levels of specific pectin domains that were solubilized with each extractant (Figure 8). A substantial additional amount of LM19 positive material was solubilized by water and CDTA in the cell wall preparations from the *TBG4* mutants in comparison to the other genotypes (Figure 8A). However, significantly ($P<0.05$) more de-esterified HG was retained in the cellulose residue in the absence of PL, PG2a or TBG4 in comparison to wild type controls where all three enzymes were present (Figure 8A). The LM5 response was significantly ($P<0.05$) higher in all fractions in the *TBG4* fruit extracts and reduced most in the *PG2a* lines with polysaccharides extracted with water, CDTA and KOH (Figure 8B). Galactan-rich pectins were retained with the cellulose residue in the absence of *PL* and *TBG4* activity (Figure 8B).

As part of the cell wall extraction experiments we tested two additional antibody probes to those used in the immunocytochemistry studies. The INRA-RU1 monoclonal antibody (Ralet et al., 2010) recognises the RG-I backbone. Significantly ($P<0.05$) less backbone RG-I epitope was solubilized with water when *PL* and *PG2a* were silenced in comparison to the wild type lines and the *TBG4* genotype. Conversely, cellulase treatment of residues indicated that more RG-I was associated with cellulose in the absence of PL and PG2a (Figure 8C). Similarly, for the arabinan epitope of RG-I detected by LM6 (Figure 8D), lower levels of epitope were solubilized in water and CDTA in the absence of PG2a and higher levels relative to wild type were detected in the cellulase-extracted fraction (Figure 8D). The use of a post-alkali cellulase treatment to release pectic fractions provides an insight into the potential importance of cellulose microfibril associated pectins.

DISCUSSION

Recent advances in DNA editing have made it possible to precisely manipulate plant genomes. The CRISPR/Cas9 system has been utilised successfully for mutagenesis in a variety of organisms including plants such as Arabidopsis (Gao et al., 2016), rice (Xu et al., 2015; Sun et al., 2016), wheat (Wang et al., 2014), maize (Svitashev et al., 2016). In tomato, genes that have been targeted include *SlAGO7* (Brooks et al., 2014), *RIN* (Ito et al., 2015), *SlPDS* and *SlPIF4* (Pan et al., 2016), *DELLA* and *ETR1* (Shimatani et al., 2017). Here, we have shown that CRISPR/Cas9 can induce mutations in the genes *PL* (*Solyc03g111690*), *PG2a* (*Solyc10g080210*) and *TBG4* (*Solyc12g008840*) that encode pectin degrading enzymes. In our study, the CRISPR mutations resulted in a range of transcript abundance with only PG2a showing substantial reductions in transcript levels (Figure S4). In eukaryotes, selective mRNAs containing a Premature Translation Termination Codon (PTC) are targeted for degradation by Nonsense-Mediated mRNA decay (NMD) (Lykke-Andersen and Jensen, 2015) and often associated with decreased mRNA levels compared with their counterparts without premature translation termination codon PTC. Both *PG2a* mutant lines have frame-shifts resulting in stop codons being introduced early within the transcript. As such, they are likely to be targets of the NMD. The *PG2a* mRNA is one of the most abundant transcripts during normal ripening and this is in part due to its unusually long half-life rather than a particularly high transcription rate (DellaPenna et al., 1989). A switch to rapid turnover as a result of becoming an NMD target will thus have a proportionately stronger impact on the *PG2a* mRNA steady state levels.

All the modified sequences at our target sites were predicted to generate stop codons and subsequent measures of enzyme activity indicated the CRISPR mutations eliminated the target functions. Interestingly low ripening-related activities for PL, PG, and TBG were apparent and this residual activity likely reflects the expression in the fruit pericarp of other members of the respective gene families. For example, qPCR data indicates that other *PL* and *PG* genes are being upregulated to some extent to compensate for mutations in the main ripening-expressed gene family members (Figure S5).

CRISPR mutations targeting pectin degrading enzymes and the impact on ripening

Prior to the development of DNA editing technology, antisense RNA and RNAi lines had been generated to silence *PG2a*, *PL* and *TBG4* (Sheehy et al., 1988; Smith et al., 1988; Uluisik et al., 2016; Yang et al., 2017; Smith et al., 2002). *PG2a* antisense lines showed no effects on

fruit texture, although pectin depolymerisation was inhibited (Smith et al., 1990). The *TBG4* antisense lines yielded fruit that were reported to be somewhat firmer than those of the control line (Smith et al., 2002). More recently RNAi lines suppressing *PL* expression resulted in marked effects on tomato fruit texture (Uluisik et al., 2016; Yang et al., 2017).

In the current study, using *cv. Ailsa Craig* tomato fruits, only the silencing of *PL* resulted in any measurable effect on fruit softening in contrast to previous reports relating to *TBG4*. The differences between our work and effects on the *TBG4* antisense fruits reported by Smith et al., (2002) could be due to the genetic background as they performed their experiments in the *c.v. Rutgers*. The ability of reduced PL activity to delay softening, without impacting other aspects of ripening, was reported in both *cvs Ailsa Craig, M82* (Uluisik et al., 2016) and *Micro-Tom* (Yang et al., 2017) indicating a key role for this gene in modulating softening in cultivated tomato (*Solanum lycopersicum*). Interestingly fruits of the *PG2a* and *TBG4* CRISPR lines showed altered colour and weight. It has been suggested that pectin oligomers and sugar residues such as galactose, generated by cell wall degradation, could be involved in initiating the ripening process, possibly through induction of ethylene biosynthesis (Gross, 1985; Melotto et al., 1994).

Carotenoid analysis indicated that the changes in pericarp colour in the *TBG4* and *PG2a* lines was due to altered β-carotene and lycopene content. A profile of increased β-carotene with a concurrent reduction in lycopene indicates that ripening related carotenoid formation has been altered possibly through the modulation of lycopene beta-cyclase (beta-LCY) activity. This enzyme converts lycopene to β-carotene and is normally down-regulated at the breaker stage of fruit development (Pecker et al., 1996). In the *PL* CRISPR lines, some pectin degradation may occur due to the activity of the normal *PG2a* and *TBG4* gene products. The delayed colour development in the *PG2a* and *TBG4* lines could, therefore, reflect a delay in the onset of ripening. The observed alteration in carotenoid profiles may reflect changes in ethylene perception or response. There was no strong evidence that the differences in fruit weight in the *PG2a* and *TBG4* lines were due to altered water relations in the fruits based on fresh weight to dry weight ratios in the pericarp. Also there was is no strong evidence that the fresh weight to dry weight ratio in the PL lines differed from that of the wild type, which was consistent with them both having a similar water content. The difference in fruit weight seen in the *PG2a* and *TBG4* lines merits further investigation.

Previous studies have reported that in tomato, juice produced from transgenic fruit with reduced PG2a activity, using antisense technology, was thicker and had a higher viscosity (Schuch et al., 1991; Errington et al., 1998). The properties of tomato juice or paste differ between varieties and are likely to reflect differences in cell wall physiochemical properties between the genotypes (Thankur et al., 1996). Tomato paste is composed of suspended particles including whole cells, broken cells and cellular fragments in an aqueous serum. In this work, the higher viscosity of the pastes made from the *PL* and *PG2a* CRISPR lines are likely explained by changes in pectin molecular size resulting from reduced pectin degradation as a result of the silencing of these genes (Uluisik et al., 2016). The similarity between *PL* and *PG2a* CRISPR fruits with respect to paste viscosity is consistent with an effect on polyuronide molecular weights rather than pectin solubility, which is unaffected in low *PG2a* antisense fruits (Smith et al., 1990), but inhibited in PL CRISPR lines (Uluisik et al., 2016). Rheological characterisation of juices obtained from transgenic *PL*-silenced strawberry fruits suggested increased content of large particles in juice and the enhanced viscosity were the result of silenced PL activity and the improved tissue integrity (Sesmero et al., 2009).

Pectin localisation, degradation and tomato fruit softening

The antibody probe LM19 recognises de-esterified HG. In the *PL* CRISPR mutants, which would be expected to have normal PG2a and TBG4 activity, intense staining of both the ML and tricellular junction zones was apparent. The *PG2a* CRISPR fruits showed ubiquitous LM19 labelling throughout their cell walls including the ML region, tricellular junction zones, and even the intercellular spaces. This was in contrast to the control fruits where some labelling of the primary wall was apparent, but HG appeared absent from other areas. These data support previous findings (Uluisik et al., 2016) that PL is especially important in degrading de-esterified HG at tricellular junctions and it has been reported in other plant tissues that the tricellular junction zones are rich in de-esterified HG (Willats et al., 2001).

The immunolocalisation studies indicated that the presence of both normal PG and PL enzymes was necessary to degrade pectin to the extent seen in the wild type fruits. These data are consistent with previous reports that in tomato pectin solubilisation requires PL, but PG2a is important for full pectin depolymerisation (Smith et al., 1990; Uluisik et al., 2016). Interestingly in the absence of TBG4 activity in the *TBG4* CRISPR lines, but with *PG2a* and *PL* expression present, the LM19 labels predominantly the primary cell walls, with some labelling of the ML, tricellular junctions and no labelling of the intercellular spaces. This

indicates that PG2a and PL are necessary and sufficient to degrade de-esterified HG in the junction zones. Moreover, the galactanase encoded by *TBG4* is needed for full solubilisation of de-esterified HG in the ML and primary cell wall, which must be rich in HG and HG linked to RG-I, harbouring sidechains of β1,4-galactan.

The LM5 probe, that detects β1-4-galactan, showed limited labelling in the ML region in the control, *PL* and *PG2a* CRISPR fruits, which indicates that even in the absence of PL or PG2a, galactans are solubilized from the cell wall and especially the ML. A role for PL in this process was apparent when LM5 labelling of the *PL* CRISPR cell walls was undertaken. There was intense LM5 labelling of the cell walls of both *PL* and *TBG4* mutants. This indicates PL is necessary to facilitate the normal degradation of β1-4-galactans and as might be expected the absence of the TBG4 gene product impacts the solubilisation of these polymers and likely RG-I. De-esterified HG has an important role in plant cell wall structure occurring at points of cell separation such as tricellular junctions and in the ML (Willats et al., 2001) by mitigating forces that drive cell separation.

A consistent feature of the parenchyma cells in the *TBG4* CRISPR lines was that the intercellular spaces and junction zones appeared larger and more separated than in the *PL* and *PG2a* CRISPR lines and even the control fruits. A possible explanation for this observation is that in the *TBG4* CRISPR lines, active *PL* and *PG2a* enzymes will have degraded de-esterified HG in the cell junctions and ML regions, but RG-I associated β1-4-galactans have remained intact. These β1-4-galactans are thought to reduce flexibility in plant cell walls. For instance, compression tests on pea cotyledons have revealed that galactan-rich cell walls were twice as stiff as those without detectable galactan-rich RG-I (McCartney et al., 2000; Bidhendi and Geitmann, 2016). Therefore, in the absence of HG at tricellular junctions, the presence of galactans in the primary wall may result in elevated levels of separation at the junction zones. This enhanced cell separation may counter-balance the impact of the loss of *TBG4* on fruit firmness. This could explain the variation between the effects of silencing *TBG4* in different tomato backgrounds as cell wall remodelling changes will likely vary between genotypes depending on the levels of PL, PG2a and other pectin degrading enzymes.

To complement the immunocytochemical studies, we investigated the classes of pectin that could be extracted from cell wall material of the different genotypes using a range of solvents. Previous studies indicated that total water-soluble pectin levels are affected by silencing PL

(Uluisik et al, 2016), but silencing PG has limited effects on pectin solubilisation (Smith et al, 1990). In the present study, we wanted to focus on specific pectin domains to provide more detailed information on the changes in these polysaccharides in mutant and wild type fruits. The pectin solubilized from the cell wall material was characterised with the same monoclonal antibody probes as for the immunomicroscopy, LM19 and LM5 and two additional probes, INRA-RU1 and LM6 recognising the RG-I backbone and arabinan epitopes respectively. For de-esterified HG that had become water soluble, LM19 detected elevated levels in the *TBG4* fruits. Furthermore, these fruits showed enhanced levels of galactan-rich pectin in the water soluble fractions. These data may reflect the increases in cell separation observed in the *TBG4* fruits as pectin solubility, cell wall swelling and presence of intercellular spaces have been linked (Redgwell et al, 1997).

The results of the cell wall analysis were consistent with the immunomicroscopy and demonstrated varying degrees of increased retention (reduced solubility) of HG and galactan-rich pectin in the *PL*, *PG2a* and *TBG4* lines in comparison to wild type fruits. There was a significant reduction in the solubility of RG-I and the associated galactan and arabinan epitopes associated with the cellulose residue in all the mutants, and less INRA-RU1 epitope was water soluble in the *PL* and *PG2a* lines. Published studies on cellulose composites and cellulose microfibrils have indicated that an elevated neutral sugar content of pectin increases its ability to bind to cellulose and pectin has been observed to accumulate in the spaces of the fibrillar network, as well as adjacent to fibrils. Pectin is likely to coat cellulose microfibrils and affect their level of aggregation (Lin et al., 2016). Cellulose and pectin together have been shown to contribute to the load-bearing capacity of composites during compression. The changes in cellulose microfibril domain structure are likely important in wall toughness and developmental changes including growth (Thomas et al., 2013; Lin et al., 2016), and this may also be the case in fruit ripening.

The importance and role of pectin in cell wall structure is undergoing something of a renaissance. In the generally accepted ‘tethered network’ hypothesis (Carpita and Gibeaut, 1993) the main structural component of the primary cell wall was postulated to be the cellulose microfibrils tethered by hemicellulose molecules. Pectin was thought to form a further independent network with so-called ‘egg box’ structures, in which divalent calcium ions cross-linked chains of demethylesterified HG. Recent studies have indicated, however, that pectin may be much more closely associated with cellulose microfibrils than previously thought.

Using solid-state nuclear magnetic resonance spectroscopy (ssNMR) of ^{13}C labeled Arabidopsis cell walls it has been demonstrated that pectin-cellulose interactions are extensive and pectin galactan chains may intercalate within, or between, nascent cellulose microfibrils during their synthesis (Dick-Pérez et al., 2011; Wang et al., 2012; Wang et al., 2015; Wang and Hong, 2016). In addition, pectin structure may also involve features that have received little attention in relation to their role in the cell wall such as branching of the main galactosyluronic acid backbone (Round et al, 2010).

The role of HG in cell adhesion and the close association of pectic galactans (RG-I) with cellulose microfibrils is entirely consistent with the observations on the CRISPR mutants made in this study. PL and also the galactanase encoded by *TBG4* are necessary for changes in the primary cell wall and ML degradation seen in normal ripening. These changes include the tight control of cell separation which is enhanced if galactan-rich pectin remains associated with the primary cell wall after degradation of de-esterified HG by PL and PG2a.

The loss of galactose residues associated with the cellulose fraction of cell walls from ripening fruits was observed many years ago (Seymour et al., 1990). The present study supports a model where the pectin degrading enzymes act in a hierarchy to solubilize de-esterified HG and RG-I leading to tight control of fruit softening and cell separation. We propose that in tomato, PL acts on insoluble high molecular weight pectic polysaccharides that are associated with cellulose at cell junctions and also on pectin in the ML. The effects of PL involve disaggregation and depolymerisation of de-esterified HG (Uluisik et al., 2016). In combination with the action of the galactanase, encoded by *TBG4*, HG and RG-I are further solubilized and then HG is depolymerised by PG2a (Smith et al, 1990). Eventually these processes lead to cell separation.

In contrast to tomato, strawberry softening is inhibited to a much greater degree by removal of PG activity (Posé et al., 2015). In this fruit, PG seems to be more active than PL on highly branched pectin in the cell wall. Also, in strawberry, silencing of a cell wall β-galactosidase resulted in firmer fruits (Paniagua et al., 2016). The reason for this variation between species is unclear, but may reflect differences in cell wall composition or the levels of other additional wall modifying activities that include remodelling of the interactions between pectin and other wall components, such as cellulose, which have often been ignored in previous studies. This may also explain why the effects of silencing of specific genes such as *TBG4* depends on the

tomato genetic background. This is illustrated by the observation that in *cv. Rutgers TBG4* down-regulation impacts fruit softening (Smith et al., 2002), while mutations in this gene were unable to influence texture changes in *cv. Ailsa Craig* in the present study. These results emphasise the complexity of cell wall remodelling and its effects on plant phenotypes.

MATERIALS AND METHODS

Construction of Cas9/sgRNA expressing vectors

The sites used for targeted mutagenesis were designed according to (Shan et al. 2014) using the CRISPR-PLANT tools and the tomato genome sequence database (www.solgenomics.net; Tomato Genome Consortium, 2012) and are listed in Table S1. The construction of AtU6p::sgRNA vector and the Cas9/sgRNA expressing vectors were based on Golden Gate cloning technology. The sgRNAs were amplified using primers described in Supplementary Table S4 using the plasmid pICH86966:: AtU6p::sgRNA PDS construct (Addgene plasmid 46966) as a template. sgRNAs placed under the Arabidopsis U6 promoter were cut-ligated with the pICSL01009::AtU6p level 0 (Addgene#46968) module into pICH47751 level 1 vector (Addgene #48002) using the Golden Gate cloning method (Weber et al., 2011). sgRNA-Cas9 plant expression vectors were constructed by performing cut-ligation reaction with Level 1 modules pICH47732::NOSp::NPTII (Addgene #51144), pICH47742::35S::Cas9 (Addgene #49771), pICH47751::AtU6p::sgRNAs and the linker pICH41766 (Addgene # 48018) into the level 2 Golden Gate vector pAGM4723 (Addgene #48015) using BbsI as described by Weber et al., 2011. The complete sequence of nptII-Cas9-sgRNA expression cassette was sequenced to verify that the clones had the correct transgene.

Plant materials, growth conditions, and generation of transgenic plants

The Cas9/sgRNA constructs were transformed into *Agrobacterium* strain EHA105 by electroporation. *Agrobacterium tumefaciens*-mediated transformation of tomato cultivar *Ailsa Craig* were performed according to McCormick (1991). Plantlets were acclimated to become sturdy plants before transfer to the harsher conditions of glasshouse. All tomato lines were grown in the UK under standard glasshouse conditions of 16-h day length and 25 °C, with night a temperature of 18 °C. Supplemental lighting provided where required. Plants from each genotype were grown in “CNSC” coarse potting compost (Levington) in 7.5 L pots with

irrigation supplemented with Vitax 214 with pot locations randomized throughout the glasshouse.

Transgenic verification, genotyping and segregation of targeted mutagenesis in T_1 generation

Leaflets were collected from each T_0 plant and genomic DNA was extracted using ISOLATE II Plant DNA Kit (BIOLINE). The presence of Cas9/sgRNA transgene was verified by PCR with primers pAGM4723 F3/R3 (Table S5) designed to amplify a region spanning a 1652bp coding region of Cas9. To detected CRISPR/Cas9-induced mutations, the genomic regions surrounding target sites were amplified using specific PCR primers (Table S5). The fragments were directly sequenced or cloned into the pJET1.2/blunt vector and sequenced. The genotypes were also examined to investigate the transmission pattern of CRISPR/Cas9-mediated mutations. T_1 progeny were obtained by strict self-pollination. For each T_0 line, 10-20 progeny were randomly selected and examined by sequencing.

Quantitative RT-PCR

Total RNA from tomato fruit pericarp at breaker+7 was extracted with Spectrum TM Plant Total RNA Kit (Sigma-Aldrich). 500ng total RNA was reverse-transcribed into 20µl complementary DNA (cDNA) using SuperScript™ III First-Strand Synthesis SuperMix (Invitrogen) following the manufacturer's instructions. The qPCR amplification was carried out using PerfeCTa SYBR Green SuperMix (Quanta Biosciences). A 10µl reaction mixture was set up and contained 5µl PerfeCTa SYBR Green SuperMix (2X), 0.3µl forward/reverse primer (10uM) and an input quantity of cDNA corresponding to 0.25ng of total RNA with ddH_2O. Four experimental replicates were performed for each sample. RT-PCR was run on a LightCycler480 System (Roche Applied Science); PCR conditions were as follows: an initial denaturation step at 95 °C for 10 min, followed by 45 cycles of 95 °C for 15 s, 60 °C for 60s; a final cooling step at 40 °C for 10 min. Elongation factor 1-alpha gene (EF-1 α) was used as internal control. Gene-specific primers for RT-qPCR are listed in Table S6. The relative expression levels were calculated using the relative standard curve method and expressed as the relative quantity of target normalized to the reference gene EF-1a.

Physiochemical analysis and mechanical measurement of fruit texture

Fruit color index was recorded using a Minolta colorimeter CR400. Readings were taken based on the L*, a* and b* Hunter colour scale and colour index (CI) value was calculated from the equation CI= $(2000 \cdot a^*)/ [L^* \cdot (a^{*2}+b^{*2})^{1/2}]$ (López Camelo and Gómez, 2004). Soluble solids were recorded as % Brix and measured by a hand-held refractometer. The mechanical properties of fruit were measured using probe penetration tests using a Lloyd Instrument LF plus machine equipped with a 10 N load cell and 1.6-mm flat-head cylindrical probe as described by Uluisik et al. (2016). Measurements were taken separately from the outer and inner pericarp in duplicate.

Viscosity analysis of tomato paste

The tomato fruit was peeled and halved. Seeds and locular tissue were removed and the pericarp which was ground in a coffee machine for 30 seconds to make the puree. Stirred viscosity was measured at 20 °C based on a-20ml volume of puree using a RheoLabQC Quality Control Rheometer installed with the Rheoplus software according to the manufacturer's instructions (Device: RheolabQC SN910545; FW1.24; Application: RHEOPLUS/32 Multi3 V3.40 21004817-33028; Measure system: CC27/S-SN18049; d=0 mm). For each sample, viscosity was measured against a range of shear rates changing from 1 to 100 [1/s] on a logarithmic setting at 11 measurement points. [measuring profile: shear rate d(gamma)/dt = 1 ... 100 1/s log; |Slope| = 5 Pt. / dec].

Determination of polygalacturonase (PG) activity, β-galactosidase activity and β-galactanase activity

Enzyme extracts were made from 5g of frozen pericarp sampled at breaker+7 stage following the methods described by Pressey (1983). Frozen tomato pericarp tissue was ground with a coffee grinder into fine powder. All subsequent steps were conducted at 4 ^oC. This powder was then homogenized with 20ml ddH_2O and the suspension was stirred for 30min. Solid NaCl was added to a final concentration of 1.0 M and pH was adjusted to 6.0 with 1.0 M NaOH. The suspension was then stirred for an additional 1 h. The supernatant was collected after centrifugation at 8000g for 20 min and ammonium sulphate was added to 80% of saturation. Protein was allowed to precipitate overnight and collected by centrifugation at 16000g for 30min. The pellet was re-suspended with 2 ml 80% ammonium sulphate. Protein concentrations of crude enzyme solution were measured by the Bradford method (Bradford, 1976) using Quick Start™ Bradford Protein Assay Kit (Bio-Rad).

Determination of PG activity was based on the analysis of reducing groups released from polygalacturonic acid substrate (Honda et al., 1982). β -Galactosidase activity was assayed by measuring the rate at which it hydrolyzed p-nitrophenyl-p-D-galactopyranoside (Pressey, 1983). β-galactanase (Exo-galactanase) was assayed by measuring the release of monomeric D (+) galactose in reducing group against a potato pectic galactan pretreated with arabinofuranosidase (Megazyme, Wicklow, Ireland) following previously described methods (Carey et al.,1995).

Determination of PL enzyme activity

PL activity was estimated by the method described in Uluisik et al, (2016) and based on Collmer et al (1988). For preparation of the acetone insoluble solids (AIS), 20g of fresh pericarp (breaker+7) was homogenised with cold 80% of acetone. The sample was washed with 100% acetone to remove all pigment and the powder left overnight to dry at room temperature. Then 5 mg of the AIS was stirred for 30 min in 1.9 ml of 8.5 M Tris-HCL at 20^{o}C. The samples were then centrifuged for 30 minutes at 14000 rpm, and the absorbance of clear supernatant was measured at 232 nm, for determination of the level of reaction products with double bonds released as a result of PL activity. Controls were conducted using a parallel assay where the AIS was inactivated by boiling in 80% ethanol.

Carotenoid analysis

Carotenoids were extracted from 10 mg freeze dried fruit as described in Fraser et al.,(2000) by the addition of chloroform: methanol: water (2:1:1). Phase separation was facilitated by centrifugation of mixture and the organic phase containing carotenoids was collected and taken to dryness under vacuum centrifugation (Genevac EZ.27). Dried samples were stored at -20°C and re-dissolved in ethyl acetate prior chromatographic analysis.

Carotenoids were separated and identified by Ultra High Performance Liquid Chromatography with photo diode array detection (UPLC-PDA) as previously described (Uluisik et al, 2016). An Acquity™ UPLC (Waters) was used with a BEH C18 column (2.1 x 100 mm, 1.7 µm) with a BEH C18 VanGuard pre-column (2.1 x 50 mm, 1.7µm). The mobile phase used was A: MeOH/H2O (50/50) and B: ACN (acetonitrile)/ethyl acetate (75:25) at a flow rate of 0.5 ml/min. All solvents used were HPLC grade and filtered prior to use through a 0.2µm filter. The gradient was 30% A: 70% B for 0.5 min and then stepped to 0.1% A:99.9% B for 5.5 min

and then to 30% A:70% B for the last 2 min. Column temperature was maintained at 30°C and the samples' temperature at 8°C. On-line scanning across the UV/Vis range was performed in a continuous manner from 250 to 600 nm, using an extended wavelength PDA (Waters). Carotenoids were quantified from dose-response curves of authentic standards.

Immunofluorescence and immunocytochemistry procedures

For immunofluorescence microscopy, tomato fruit were harvested at breaker + 4 from a range of CRISPR lines and azygous controls. 2-mm cubes of pericarp tissue cut from the equatorial sections were fixed in 0.1 M sodium cacodylate buffer, 2% paraformaldehyde, pH 6.9 overnight at 4°C. Samples were dehydrated by incubation in an ascending ethanol series (30, 50, 70, 90, and 100%) with 1 h incubation for each change at 4°C. Dehydrated cubes were then infiltrated with resin at 4°C by increasing from 25% resin in ethanol for 2 h, to 50% overnight and then 75% for 8h and 100% resin overnight. This was followed by a further four changes of absolute ethanol/LR White resin mix. Samples were then placed in 8 mm flat bottomed TAAB embedding capsules (C094, TAAB) containing LR White Resin and allowed to polymerize at 60°C for 9h. Then blocks were trimmed and 0.5-µm sections were cut using a Diatome Ultra 45° diamond knife on a Leica EM UC7 ultramicrotome and collected onto 6.7 mm ten-well cavity diagnostic slides (Thermo scientific) precoated with 2% (3-aminopropl) triethoxysilane in acetone.

For the *in situ* labelling procedures rat monoclonal antibodies LM19 to unesterified HG (Verhertbruggen et al. 2009) and LM5 to 1,4-galactan (Jones et al. 1997; Andersen et al. 2016) were used. Non-specific binding was blocked with 3% (w/v) solution of fat-free milk powder in phosphate-buffered saline (PBS/MP) for at least 30 min and sections were washed PBS for 5 min. Specimens were incubated with a tenfold dilution of primary monoclonal antibody diluted in PBS/ MP for 2 h at room temperature. They were then washed with three changes of PBS with at least 5 min for each change. After the incubation, they were incubated with a secondary antibody anti-rat IgG (whole molecule)-FITC (Sigma F1763) diluted in a 100-fold in PBS/MP for 1.5h at RT and washed with three changes of PBS with at least 5 min for each change. Samples were mounted using a small drop of Citifluor AF1 glycerol/PBS-based anti-fade mountant solution (Agar Scientific). Coverslips (22x50mm, NO 1.5) were sealed with nail polish. The specimens were examined with a Leica TCS SP5 Confocal Laser Scanning Microscope according to user guide and micrographs were analysed with the Image J software.

For quantitative assessments of pectic epitopes in sequentially solubilized cell wall fractions rat monoclonal antibody LM6 to arabinan (Willats et al. 1998) and mouse monoclonal antibody INRA-RU1 to the backbone of RG-I (Ralet et al. 2010) were used in addition to LM19 and LM5. Cell wall material where endogenous pectin degrading enzymes were inactivated was prepared as follows. Tomato pericarp was frozen in liquid N_2 and broken into small pieces in a pestle and mortar. The cubes were then boiled in 95% EtOH (100 mL) at 80°C for 30 min. The sample was cooled to room temperature, homogenised using a Polytron Homogenizer and then filtered through Miracloth and washed successively with hot 85% EtOH (200 mL), chloroform/methanol (1:1 v/v) (200 mL) and 100% acetone. The samples were then air dried overnight. This crude cell wall preparation was then used in the fractionation studies. The cell wall materials were sequentially extracted (10 mg in 1 ml) with water, CDTA, 4 M KOH and with a cellulase treatment of the final insoluble residue to release polysaccharides associated with cellulose microfibrils as described (Posé et al. 2018). Solubilised extracts at dilutions ranging from 250-fold to 31250-fold were used to coat microtitre plates prior to ELISA procedures as described (Willats et al. 1998; Posé et al. 2018).

Transmission Electron Microscopy (TEM)

70nm thick sections were cut from resin blocks previously prepared for immunohistochemistry using a Diatome Ultra 45° diamond knife on a Leica EM UC7 ultramicrotome, and collected onto 3.05mm copper mesh grids (Agar Scientific). Grids were contrasted for 30 minutes in 2% Uranyl acetate and washed in pure water, followed by 5 minutes in Reynolds lead citrate, washed in pure water and allowed to dry. Samples were imaged in a JEOL JEM-1400 TEM with an accelerating voltage of 100kV. Images were captured using a Megaview III digital camera with iTEM software.

Statistical Analysis

There were replicate plants from each genetic line. For each parameter, the variation among plants was partitioned by Analysis of Variance into the variation between and within genetic lines and the residual variation among plants of the same genetic line was used as the pooled variance estimate for subsequent post-hoc pairwise comparisons between means. Dunnet's test was applied when the objective was to compare each mutant line mean to the mean of the wild type control and Duncan's multiple range test when all possible pairs of means were to be compared.

Figure Legends

Figure 1: Generation of a range of CRISPR alleles in *PL*, *PG2a* and TBG4. The mutations generated in specific regions of gene coding sequences are shown. The region for the single guide RNA sequences are in red and insertions in blue. Deletions are indicated by a dotted line. The PAM site is show in yellow.

Figure 2: The effect of the CRISPR mutations in the tomato PL, PG2a and TBG4 genes on the activity of the enzymes that they encode. (A) PL activity was estimated in the acetone insoluble fraction containing cell wall pectin. There were two independent CRISPR PL lines, (B) PG2a activity was determined by release of reducing groups and there were three Independent CRISPR lines and (C) β-galactanase activity as release of galactose residues with two independent CRISPR lines. For PG2a and galactanase enzyme activity is expressed as per μ or mg protein basis respectively. Error bars are ±SEM, n=3. Significant differences between CRISPR lines and the control are denoted by *** ($P<0.001$) based on a Dunnett's test.

Figure 3: Effect of CRISPR mutations on fruit pericarp texture. The texture of the pericarp of the different CRISPR lines was compared by measurement of maximum load. There were two *PL*, three *PG2a* and two independent *TBG4* lines respectively. At least 5 biological replicates (individual fruits from different plants) were measured for texture from each line. Significant ($P<0.05$) differences between a line and the control determined by a Dunnett's test are denoted by *. Error bars are ±SEM.

Figure 4: Effect of CRISPR mutations on fruit colour, weight and soluble sugars. Measurements were made of (A) pericarp colour, (B) fruit weight and (C) Brix levels. There were two PL, three PG2a and two independent TBG4 lines respectively. At least 5 biological replicates (individual fruits from different plants) were measured from each line. Significant ($P<0.05$) differences between a line and the control based on a Dunnett's test are denoted by *. Error bars are ±SEM. n is 5 or more.

Figure 5: Changes in viscosity of juice generated from CRISPR lines. Stirred viscosity of fruit juice was measured against sheer rates of 1 and 15.8 [1/s] using two *PL*, three *PG2*a and two independent *TBG4* lines respectively. The number of biological replicates was 3 and error bars

are ±SEM. Samples that were significantly (P<0.05) different from the control determined by a Dunnett's test are denoted by *.

Figure 6. Transmission electron micrographs of cell junctions from the pericarp of the CRISPR lines. Sections cut from three separate fruits from each of wild type, *PL5*, *PG34* and *TBG-8* lines were visualised under the transmission electron microscope and two representative micrographs shown for each line. The scale bar on each micrograph represents 10 μm. TCI = tricellular junction and PCW = primary cell wall.

Figure 7. Immunolocalisation of deesterified pectin and pectic galactan in CRISPR lines. Monoclonal antibody probes recognising deesterified pectin (LM19) and pectin associated β-galactan (LM5) were used to label tomato pericarp tissue. For each probe low (A and C) and high magnification (B and D) images are presented. Representative sections of fruits from each of wild type, PL5, PG34 and TBG-8 lines are shown. Scale bar represents 100 μm at low magnification and 10 μm at high magnification. TCJ = tricellular junction, ML = middle lamella.

Figure. 8. Extraction and characterisation of cell wall pectin fractions using pectin antibody probes. Tomato cell wall materials from three biological replicates of breaker+7 fruit pericarp of wild type (WT), PL, PG2a and TBG4 were fractionated/sequentially solubilized with water, cyclohexane diamine tetraacetic acid (CDTA), 4 M potassium hydroxide and by treatment with cellulase. The resulting sequential extracts were serially diluted and analysed with monoclonal antibodies and data for 6250x dilutions are shown. Antibodies used were (A) LM19 to un-esterified homogalacturonan, (B) LM5 to (1-4)-β-galactan, (C) INRA-RU1- to the RG-I backbone and (D) LM6 to (1-5)-α-arabinan. Levels of specific pectic polysaccharide epitopes were detected as detailed in the materials and methods. Data were analysed a Duncan's Multiple Range Test. Where significant (P<0.05) differences occur between tomato genotypes with the same extractant these are shown by different letters.

Supplemental Material

Figure S1. Amino acid sequence analysis of PL in wild type and CRISPR lines. Sequence in pink represents the polypeptide in the wild-type (WT) protein. The sequence highlighted in grey refers to an alteration in the encoded amino acid sequence in the CRISPR lines *PL5* or *PL11-1* which introduces a stop codon.

Figure S2. Amino acid sequence analysis of *PG2a* in wild type and CRISPR lines. Sequence in pink represents the polypeptide in the wild-type (WT) protein. The sequence highlighted in grey refers to an alteration in the encoded amino acid sequence in the CRISPR lines *PG34*, *PG21* or *PG1* which introduces a stop codon.

Figure S3. Amino acid sequence analysis of *TBG4* in wild type and CRISPR lines. Sequence in pink represents the polypeptide in the wild-type (WT) protein. The sequence highlighted in grey refers to an alteration in the encoded amino acid sequence in the CRISPR lines TBG4-6 and TBG4-8 which introduces a stop codon.

Figure S4. Relative expression of target genes in CRISPR mutants in *PL*, *PG2a* and *TBG4* lines. Target gene expression was measured in three fruits of each line at breaker +7 days. Error bars represent ± SEM, n=3. Significant differences between mutants and wild type control based on a Dunnet's test were marked by *** $P<0.001$.

Figure S5. Expression of *PL* and *PG2a* gene family members in the CRISPR linesmat the Breaker + 7 stage. Error bars represent ± SEM, n=5. Significant differences determined by t-test comparisons with wild type are denoted by * ($P<0.05$ *), ($P<0.01$ **), ($P<0.001$ ***).

Figure S6. β-galactosidase activity in TBG4 CRISPR lines measured as specific activity / mg of protein.

Figure S7. Carotenoid levels in the ripe fruits of the CRISPR lines. Carotenoids were extracted at Breaker +7 with three biological replicates for each line. The data were analysed to test for differences among lines using the Duncan's Multiple Range Test. Only changes in β-carotene and cis-phytoene were significant at ($P<0.05$) and are denoted by letters above the bars.

Figure S8. Calcofluor white staining of pericarp sections from CRISPR lines. Fruits from *PL5*, *PG34* and *TBG-8*. Sections show (A) outer and (B) inner pericarp. Scale bar = 100µm.

Table S1. Target sequences of cell wall structure-related genes.

Table S2. Fresh weight / dry weight ratios of pericarp sections from three independent wild type (WT) and *PG2a*, *PL* and *TBG4* lines. The overall variation among the means was not significant ($F_{3,8df}=2.76$; $P=0.111$).

Table S3. Fluorescence intensity based on analysis of sections in the confocal microscope at 10x objective with ImageJ and using Duncan's Multiple Range Test to compare lines. Values in body of table are mean intensity for each antibody probe, LM19 or LM5 ± sem, n=3.

Table S4. Primer sequences for amplifying sgRNAs.

Table S5. Primers for genotyping of CRISPR/Cas9-induced mutations.

Table S6. Primer sequences for qPCR.

ACKNOWLEDGEMENTS

Duoduo Wang was funded by a University of Nottingham Vice-Chancellor's Scholarship and the UK Engineering and Physical Sciences Research Council (EPSRC). Graham Seymour would like to thank the BBSRC and Innovate UK for financial support (grant number BB/M025918/1). The mouse RG-I antibody INRA-RU1 was kindly provided to JPK by Marie-Christine Ralet and Fabienne Guillon. We would like to thank Dr Darren Wells for his help with the confocal microscopy.

No conflicts of interest

REFERENCES

Airianah OB, Vreeburg RAM, Fry SC. 2016. Pectic polysaccharides are attacked by hydroxyl radicals in ripening fruit: evidence from a fluorescent fingerprinting method. Ann Bot. 117:441-55.

Andersen MCF, Boos I, Marcus SE, Kračun SK, Rydahl MG, Willats WGT, Knox JP, Clausen MH. 2016. Characterization of the LM5 pectic galactan epitope with synthetic analogues of β-1, 4-d-galactotetraose. Carbohydr Res. 436: 36-40.

Atmodjo MA, Hao ZY, Mohnen D. 2013. Evolving Views of Pectin Biosynthesis. Annu Rev Plant Biol. 64:747–79.

Bidhendi AJ, Geitmann A. 2016. Relating the mechanics of the primary plant cell wall to morphogenesis. J Expt Bot. 67: 449–461.

Bradford MM .1976. Rapid and Sensitive Method for Quantitation of Microgram Quantities of Protein Utilizing Principle of Protein-Dye Binding. Anal Biochem. 72: 248-254.

Brooks C, Nekrasov V, Lippman ZB, Van Eck J .2014. Efficient Gene Editing in Tomato in the First Generation Using the Clustered Regularly Interspaced Short Palindromic Repeats/CRISPR-Associated9 System. Plant Physiol. 166: 1292-1297.

Brummell DA.2006. Cell wall disassembly in ripening fruit. Funct Plant Biol. 33: 103-19

Brummell DA, Harpster MH, Civello PM, Palys JM, Bennett AB, Dunsmuir P. 1999. Modification of expansin protein abundance in tomato fruit alters softening and cell wall polymer metabolism during ripening. Plant Cell. 11: 2203-2216

Carey AT, Holt K, Picard S, Wilde R, Tucker GA, Bird CR, Schuch W, Seymour GB. 1995. Tomato exo-(1-->4)-beta-D-galactanase. Isolation, changes during ripening in normal and mutant tomato fruit, and characterization of a related cDNA clone. Plant Physiol. 108:1099-107.

Carpita NC, Gibeaut DM. 1993. Structural models of primary cell walls in flowering plants: consistency of molecular structure with the physical properties of the walls during growth. Plant J. 3:1–30

Cantu D, Vicente, AR, Greve, LC, Dewey, FM, Bennett, AB, Labavitch, JM and Powell, ALT. 2008. The intersection between cell wall disassembly, ripening, and fruit susceptibility to Botrytis cinerea. Proc. Nat. Acad.Sci. 105: 859-864

Collmer A, Ried JL & Mount MS. 1988. Assay methods for pectic enzymes. Methods Enzymol. 161: 329–335

Cornuault V, Posé S, Knox JP (2018) Disentangling pectic homogalacturonan and rhamnogalacturonan-I polysaccharides: evidence for sub-populations in fruit parenchyma systems. Fd Chem. 246:275-285

DellaPenna D, Kates DS, Bennett AB. 1987. Polygalacturonase Gene Expression in Rutgers, *rin*, *nor*, and *Nr* Tomato Fruits. Plant Physiol. 85: 502-7.

Dick-Pérez, M, Zhang Y, Hayes J, Salazar A, Zabotina OA, Hong M. 2011. Structure and Interactions of Plant Cell-Wall Polysaccharides by Two- and Three-Dimensional Magic-Angle-Spinning Solid-State NMR. Biochemistry. 50: 989–1000.

Errington N, Tucker GA, Mitchell JR. 1998. Effect of Genetic Down-Regulation of Polygalacturonase and Pectin Esterase Activity on Rheology and Composition of Tomato Juice. J Sci Food Agric. 76: 515-519.

Fraser PD, Pinto ME, Holloway DE, and Bramley PM (2000) Technical advance: application of high-performance liquid chromatography with photodiode array detection to the metabolic profiling of plant isoprenoids. Plant J. 24: 551-558.

Gao X, Chen J, Dai X, Zhang D, Zhao Y. 2016. An effective strategy for reliably isolating heritable and Cas9-free Arabidopsis mutants generated by CRISPR/Cas9-mediated genome editing. Plant Physiol. 171:1794-800.

Gross KC. 1985. Promotion of ethylene evolution and ripening of tomato fruit by galactose. Plant Physiol. 79: 306-307.

Honda S, Nishimura Y, Takahashi M, Chiba H, Kakehi K. 1982. A Manual Method for the Spectrophotometric Determination of Reducing Carbohydrates with 2-Cyanoacetamide. Anal Biochem. 119: 194-199.

Ito Y, Nishizawa-Yokoi A, Endo M, Mikami M, Toki S. 2015. CRISPR/Cas9-mediated mutagenesis of the *RIN* locus that regulates tomato fruit ripening. Biochem Biophys Res Comm. 467: 76-82.

Jiménez-Bermúdez Silvia, Redondo-Nevado J, Muñoz-Blanco J, Caballero JL, López-Aranda JM, Valpuesta V, Pliego-Alfaro F, Quesada MA, Mercado JA. 2002. Manipulation of strawberry fruit softening by antisense expression of a pectate lyase gene. Plant Physiol. 128:751-759.

Jones L, Seymour GB, Knox JP. 1997. Localization of pectic galactan in tomato cell walls using a monoclonal antibody specific to (1-4)-β-D-galactan. Plant Physiol. 113: 1405–1412

Keegstra K. 2010. Plant cell walls. Plant Physiol. 154:483–486.

Kitagawa M, Itoa H, Shiinab T, Nakamurab N, Inakumaa T, Kasumib T, Ishiguroa Y, Yabeb K, Ito Y. 2005. Characterization of tomato fruit ripening and analysis of gene expression in F_1 hybrids of the *ripening inhibitor (rin)* mutant. Physiol Plant. 123:331–338.

Klee HJ, Giovannoni JJ. 2011. Genetics and control of tomato fruit ripening and quality attributes. Annu Rev Genet. 45: 41-59.

Lin D, Lopez-Sanchez P, Gidley MJ. 2016. Interactions of pectins with cellulose during its synthesis in the absence of calcium. Food Hydrocolloids 52: 57-68.

López Camelo A, Gómez PA. 2004. Comparison of color indexes for tomato ripening. *Horticultura Brasileira.* 22: 534-537.

Lykke-Andersen S, Jensen TH. 2015. Nonsense-mediated mRNA decay: an intricate machinery that shapes transcriptomes. Nat Rev Mol Cell Biol. 16: 665–677.

McCartney L, Ormerod AP, Gidley MJ, Knox JP. 2000. Temporal and spatial regulation of pectic (1→4)-β-D-galactan in cell walls of developing pea cotyledons: implications for mechanical properties. Plant J. 22:105-13.

McCormick S. 1991. Transformation of tomato with *Agrobacterium tumefaciens*. Plant Tissue Culture Manual. B6: 311-319.

Melotto E, Greve LC, Labavitch JM. 1994. Cell Wall Metabolism in Ripening Fruit. VII. Biologically Active Pectin Qligomers in Ripening Tomato (*Lycopersicon esculentum* Mill.) Fruits. Plant Physiol. 106: 575-581.

Nekrasov V, Staskawicz B, Weigel D, Jones JDG, Kamoun S. 2013. Targeted mutagenesis in the model plant *Nicotiana benthamiana* using Cas9 RNA-guided endonuclease. Nat Biotechnol. 31: 691–693.

Pan CT, Ye L, Qin L, Liu X, He YJ, Wang J, Chen LF, Lu G. 2016. CRISPR/Cas9-mediated efficient and heritable targeted mutagenesis in tomato plants in the first and later generations. Scientific Reports. 6: 24765 doi: 10.1038/srep24765

Paniagua C, Blanco-Portales R, Barceló-Muñoz M, García-Gago JA, Waldron KW, Quesada MA, Muñoz-Blanco J, Mercado JA. 2016. Antisense down-regulation of the strawberry β-galactosidase gene *FaβGal4* increases cell wall galactose levels and reduces fruit softening. J Expt Bot. 67: 619–631.

Pecker I, Gabbay R, Cunningham FX Jr, Hirschberg J. 1996. Cloning and characterization of the cDNA for lycopene β-cyclase from tomato reveals decrease in its expression during fruit ripening. Plant Mol. Biol. 30: 807–819

Popper ZA, Fry, SC. 2005. Widespread Occurrence of a Covalent Linkage between Xyloglucan and Acidic Polysaccharides in Suspension-cultured Angiosperm Cells. Ann Bot. 96: 91–99.

Popper ZA, Fry, SC. 2008. Xyloglucan¡pectin linkages are formed intra-protoplasmically, contribute to wall-assembly, and remain stable in the cell wall. Planta. 227:781–794.

Posé S, Kirby AR, Paniagua C, Waldron KW, Morris VJ, Quesada MA, Mercado JA. 2015. The nanostructural characterization of strawberry pectins in pectate lyase or polygalacturonase silenced fruits elucidates their role in softening. Carbohydr Polym. 132:134-145.

Posé S, Marcus SE, Knox JP. 2018. Differential metabolism of pectic galactan in tomato and strawberry fruit: detection of the LM26 branched galactan epitope in ripe strawberry fruit. *Physiologia Plantarum* 164: 95–105.

Pressey R. 1983. Beta-Galactosidases in Ripening Tomatoes. Plant Physiol.71:132-135.

Quesada MA, Blanco-Portales R, Posé S, García-Gago JA, Jiménez-Bermúdez S, Muñoz-Serrano A, Caballero JL, Pliego-Alfaro F, Mercado JA, Muñoz-Blanco J. 2009. Antisense Down-Regulation of the *FaPG1* Gene Reveals an Unexpected Central Role for Polygalacturonase in Strawberry Fruit Softening. Plant Physiology 150: 1022-1032.

Ralet MC, Tranquet O, Poulain D, Moïse A, Guillon F. 2010. Monoclonal antibodies to rhamnogalacturonan I backbone. Planta 231: 1373–1383.

Redgwell RJ, MacRae E, Hallett I, Fischer M, Perry J and Harker R. 1997. *In vivo* and *in vitro* swelling of cell walls during fruit ripening. Planta 203: 162-173

Round AN, Rigby NM, MacDougall AJ, Morris VJ. 2010. A new view of pectin structure revealed by acid hydrolysis and atomic force microscopy. Carbohydr Res. 345: 487–497.

Saladié M, Matas AJ, Isaacson T, Jenks MA, Goodwin SM, Niklas KJ, Xiaolin R, Labavitch JM, ShackelKA, Fernie AR, Lytovchenko A, O'Neill MA, Watkins CB, Rose JKC. 2007. A reevaluation of the key factors that influence tomato fruit softening and integrity. Plant Physiol. 144: 1012-28.

Schuch W, Kanczler J, Robertson D, Hobson G, Tucker G, Grierson D, Bright S, Bird C. 1991. Fruit Quality Characteristics of Transgenic Tomato Fruit with Altered Polygalacturonase Activity. Hortscience. 26: 1517-1520.

Sesmero R, Mitchell JR, Mercado JA, Quesada MA. 2009. Rheological characterisation of juices obtained from transgenic pectate lyase-silenced strawberry fruits. Food Chemistry. 116: 426-432.

Seymour GB, Colquhoun IJ, Dupont MS, Parsley KR, Selvendran RR.1990. Composition and Structural Features of Cell-Wall Polysaccharides from Tomato Fruits. Phytochem. 29: 725-31

Seymour GB, Østergaard L, Chapman NH, Knapp S, Martin C. 2013. Fruit development and ripening. Annu. Rev. Plant Biol. 64:219-41

Shan QW, Wang YP, Li J, Gao CX. 2014. Genome editing in rice and wheat using the CRISPR/Cas system. *Nature Protocols.* 9: 2395-2410.

Sheehy RE, Kramer M, Hiatt WR. 1988. Reduction of polygalacturonase activity in tomato fruit by antisense RNA. Proc Nat Acad Sci USA. 85: 8805-8809

Shimatani Z, Kashojiya S, Takayama M, Terada R, Arazoe T, Ishii H, Teramura H, Yamamoto T, Komatsu H, Miura K, Ezura H, Nishida K, Ariizumi T, Kondo A. 2017. Targeted base editing in rice and tomato using a CRISPR-Cas9 cytidine deaminase fusion. Nat Biotechnol. 35:441–443

Smith CJS, Watson CF, Ray J, Bird CR, Morris PC, Schuch W, Grierson D. 1988. Antisense RNA Inhibition of Polygalacturonase Gene-Expression in Transgenic Tomatoes. Nature. 334:724-726

Smith CJ, Watson CF, Morris PC, Bird CR, Seymour GB, Gray JE, Arnold C, Tucker GA, Schuch W, Harding S, Grierson D.1990. Inheritance and Effect on Ripening of Antisense Polygalacturonase Genes in Transgenic Tomatoes. Plant Mol Biol. 14: 369-379.

Smith DL, Gross KC. 2000. A family of at least seven β-galactosidase genes is expressed during tomato fruit development. Plant Physiol. 123:1173–1183.

Smith DL, Abbott JA, Gross KC. 2002. Down-regulation of tomato beta-galactosidase 4 results in decreased fruit softening. Plant Physiol. 129: 1755-1762.

Sun YW, Zhang X, Wu CY, He YB, Ma YZ, Hou H, Guo XP, Du WM, Zhao YD, Xia LQ. 2016. Engineering Herbicide-Resistant Rice Plants through CRISPR/Cas9-Mediated Homologous Recombination of Acetolactate Synthase. Mol Plant. 9: 628–631.

Svitashev S, Schwartz C, Lenderts B, Young JK, Cigan AM. 2016. Genome editing in maize directed by CRISPR–Cas9 ribonucleoprotein complexes. Nature Comm. 13274, DOI: 10.1038/ncomms13274

Thankur B, Singh R, Nelson P. 1996. Quality attributes of processed tomato products: A Review. Food Rev.Int,12(3),375-401

The Tomato Genome Consortium. 2012. The tomato genome sequence provides insights into fleshy fruit evolution. Nature. 485: 635–641.

Thomas LH, Forsyth VT, Šturcová A, Kennedy CJ, May RP, Altaner CM, Apperley DC, Wess TJ, and Jarvis MC. 2013. Structure of cellulose microfibrils in primary cell walls from collenchyma. Plant Physiol. 161: 465–476.

Thompson JE, Fry SC. 2000. Evidence for covalent linkage between xyloglucan and acidic pectins in suspension-cultured rose cells. Planta. 211:275–286.

Tieman DM, Handa AK. 1994. Reduction in pectin methylesterase activity modifies tissue integrity and cation levels in ripening tomato (*Lycopersicon esculentum* Mill.) fruits. Plant Physiol. 106: 429–436.

Uluisik S, Chapman NH, Smith R, Poole M, Adams G, Gillis RB, Besong TMD, Sheldon J, Stiegelmeyer S, Perez L, Samsulrizal N, Wang DD, Fisk ID, Yang N, Baxter C, Rickett D, Fray R, Blanco-Ulate B, Powell ALT, Harding SE, Craigon J, Rose JKC, Fich EA, Sun L, Domozych DS, Fraser PD, Tucker GA, Grierson D, Seymour GB. 2016. Genetic improvement of tomato by targeted control of fruit softening. Nat Biotechnol. 34: 950-952.

Verhertbruggen Y, Marcus SE, Haeger A, Ordaz-Ortiz JJ, Knox JP. 2009. An extended set of monoclonal antibodies to pectic homogalacturonan. Carbohydr Res. 344: 1858-1862.

Wang D, Yeats TH, Uluisik S, Rose JKC and Seymour GB. 2018. Fruit Softening: Revisiting the role of pectin. Trends in Plant Science DOI: https://doi.org/10.1016/j.tplants.2018.01.006

Wang YP, Cheng X, Shan QW, Zhang Y, Liu JX, Gao CX, Qiu J-L. 2014. Simultaneous editing of three homoeoalleles in hexaploid bread wheat confers heritable resistance to powdery mildew. Nat Biotechnol. 32: 947–951.

Wang T, Zabotina O, Hong M. 2012. Pectin-cellulose interactions in the Arabidopsis primary cell wall from two-dimensional magic-angle-spinning solid-state nuclear magnetic resonance. Biochemistry. 51: 9846–56.

Wang T, Park YB, Cosgrove DJ, Hong M. 2015. Cellulose-Pectin Spatial Contacts Are Inherent to Never-Dried Arabidopsis Primary Cell Walls: Evidence from Solid-State Nuclear Magnetic Resonance. Plant Physiol. 168: 871–84.

Wang T, Hong M. 2016. Solid-state NMR investigations of cellulose structure and interactions with matrix polysaccharides in plant primary cell walls. J Exp Bot. 67: 503–514

Weber E, Gruetzner R, Werner S, Engler C, Marillonnet S. 2011. Assembly of Designer TAL Effectors by Golden Gate Cloning. PLoS ONE 6: e19722. doi:10.1371/journal.pone.0019722

Willats WGT, Marcus, SE, Knox JP. 1998. Generation of a monoclonal antibody specific to (1→5)-a-L-arabinan. Carbohydrate Research 308: 149-152.

Willats WG, Orfila C, Limberg G, Buchholt HC, van Alebeek GJ, Voragen AG, Marcus SE, Christensen TM, Mikkelsen JD, Murray BS, Knox JP. 2001. Modulation of the degree and pattern of methyl-esterification of pectic homogalacturonan in plant cell walls - Implications for pectin methyl esterase action, matrix properties, and cell adhesion. J Biol Chem. 276: 19404-13.

Xu R-F, Li H, Qin R-Y, Li J, Qiu C-H, Yang Y-C, Ma H, Li L, Wei P-C, Yang J-B. 2015. Generation of inheritable and “transgene clean” targeted genome-modified rice in later generations using the CRISPR/Cas9 system. Scientific Reports. 11491. doi: 10.1038/srep11491

Yang L, Huang W, Xiong F, Xian Z, Su D, Ren M, Li Z. 2017. Silencing of SlPL, which encodes a pectate lyase in tomato, confers enhanced fruit firmness, prolonged shelf-life and reduced susceptibility to grey mould. Plant Biotechnol J. 15: 1544-1555.

Yeats TH, Rose JKC. 2013. The Formation and Function of Plant Cuticles. Plant Physiology. 163: 5–20.

Figure 1: Generation of a range of CRISPR alleles in *PL*, *PG2a* and TBG4. The mutations generated in specific regions of gene coding sequences are shown. The region for the single guide RNA sequences are in red and insertions in blue. Deletions are indicated by a dotted line. The PAM site is show in yellow.

Figure 2: The effect of the CRISPR mutations in the tomato PL, PG2a and TBG4 genes on the activity of the enzymes that they encode. (A) PL activity was estimated in the acetone insoluble fraction containing cell wall pectin. There were two independent CRISPR PL lines, (B) PG2a activity was determined by release of reducing groups and there were three Independent CRISPR lines and (C) β-galactanase activity as release of galactose residues with two independent CRISPR lines. For PG2a and galactanase enzyme activity is expressed as per µ or mg protein basis respectively. Error bars are ±SEM, n=3. Significant differences between CRISPR lines and the control are denoted by *** (P<0.001) based on a Dunnett's test.

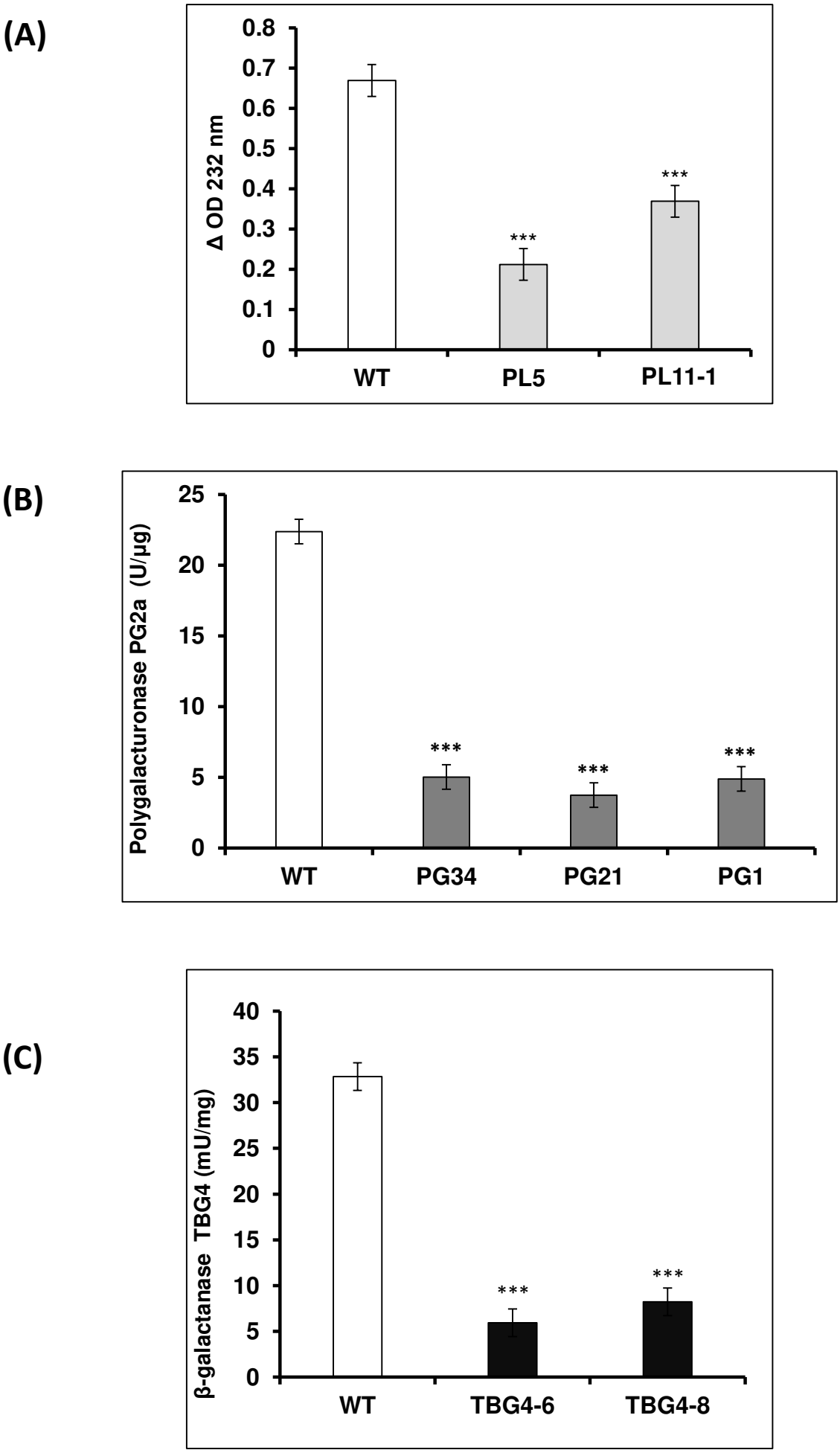

Figure 3: Effect of CRISPR mutations on fruit pericarp texture. The texture of the pericarp of the different CRISPR lines was compared by measurement of maximum load. There were two PL, three PG2a and two independent TBG4 lines respectively. At least 5 biological replicates (individual fruits from different plants) were measured for texture from each line. Significant ($P<0.05$) differences between a line and the control determined by a Dunnett's test are denoted by *. Error bars are ±SEM.

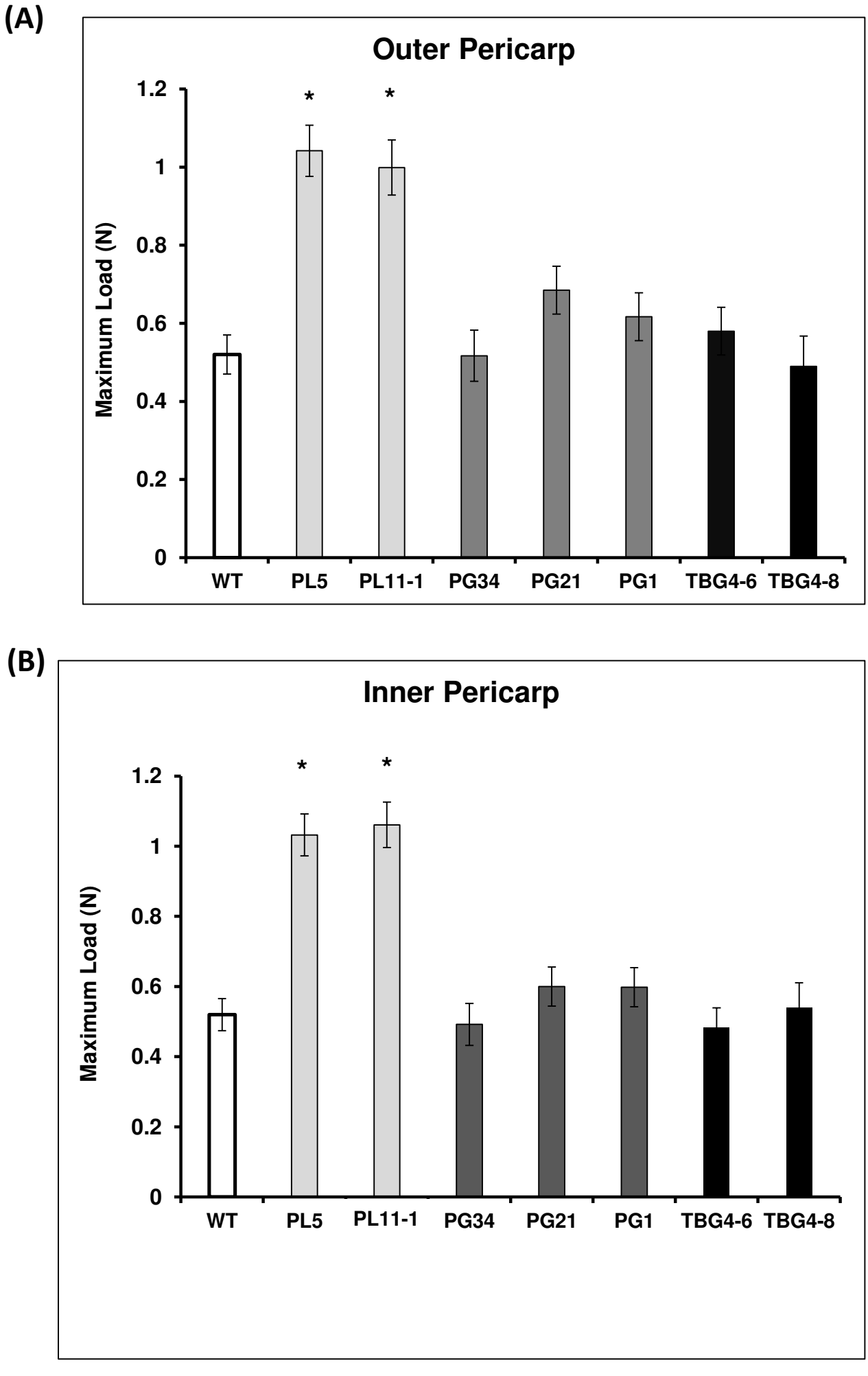

Figure 4: Effect of CRISPR mutations on fruit colour, weight and soluble sugars. Measurements were made of (A) pericarp colour, (B) fruit weight and (C) Brix levels. There were two PL, three PG2a and two independent TBG4 lines respectively. At least 5 biological replicates (individual fruits from different plants) were measured from each line. Significant ($P<0.05$) differences between a line and the control based on a Dunnett's test are denoted by *. Error bars are ±SEM. n is 5 or more.

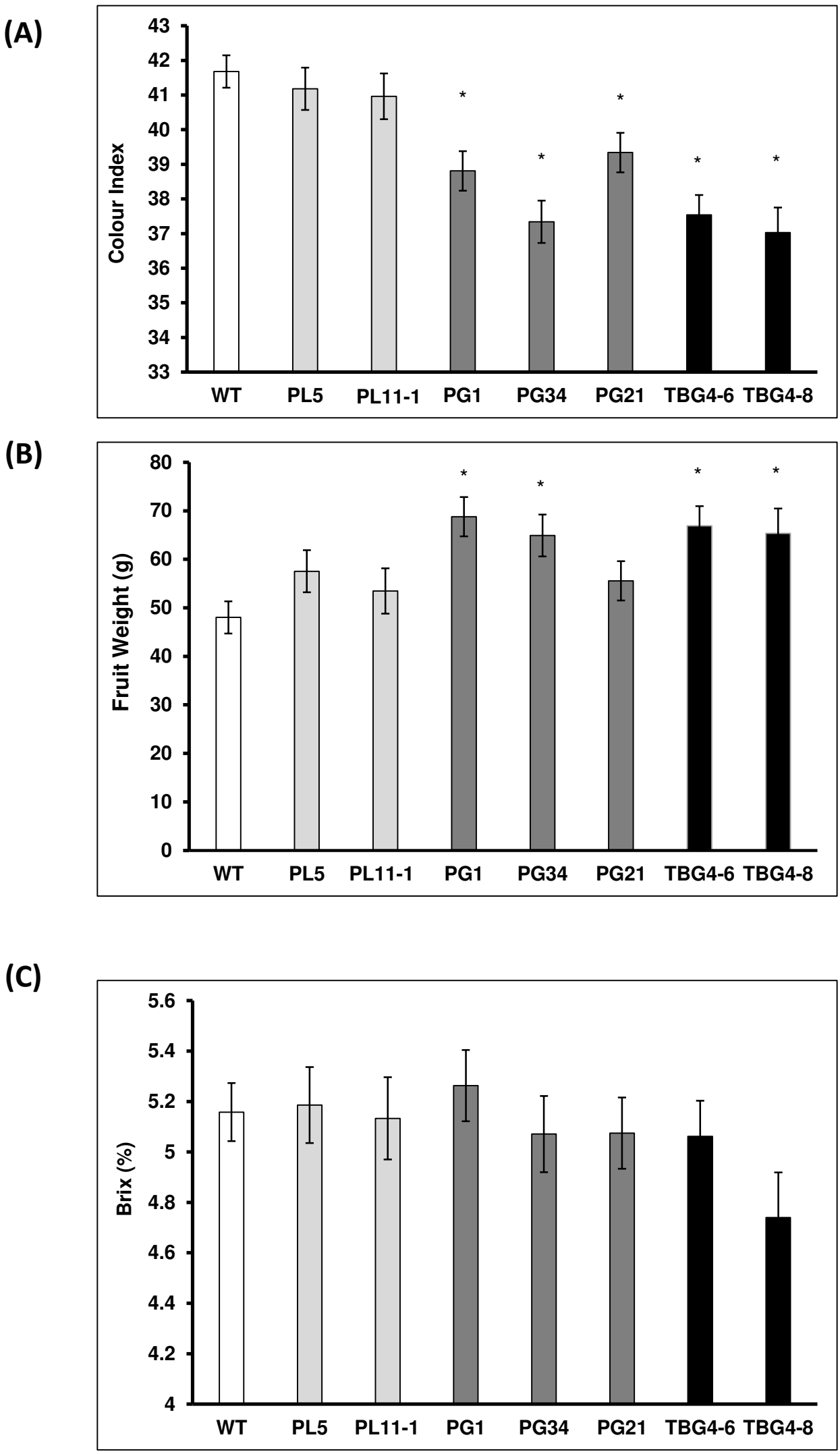

Figure 5: Changes in viscosity of juice generated from CRISPR lines. Stirred viscosity of fruit juice was measured against sheer rates of 1 and 15.8 [1/s] using two *PL*, three *PG2*a and two independent *TBG4* lines respectively. The number of biological replicates was 3 and error bars are ±SEM. Samples that were significantly (P<0.05) different from the control determined by a Dunnett's test are denoted by *.

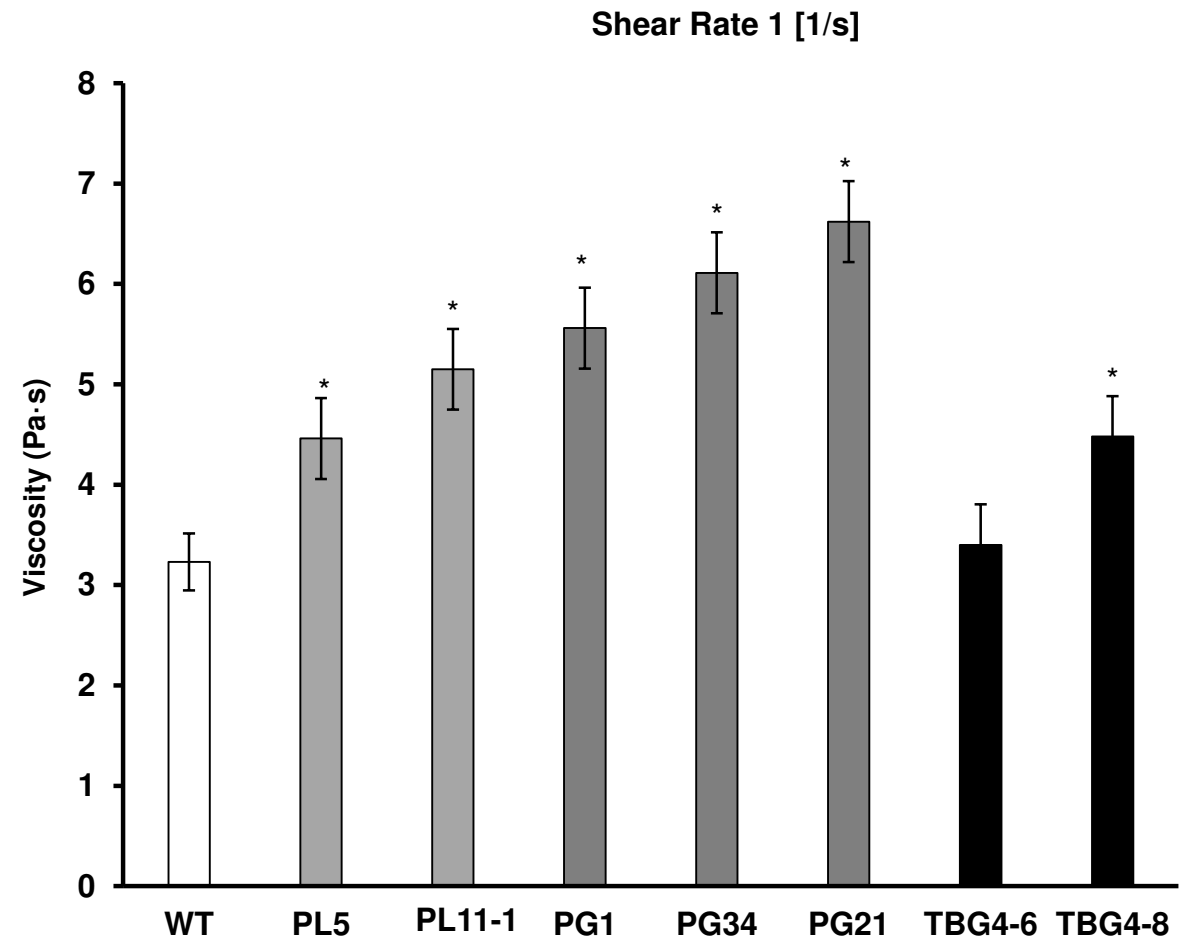

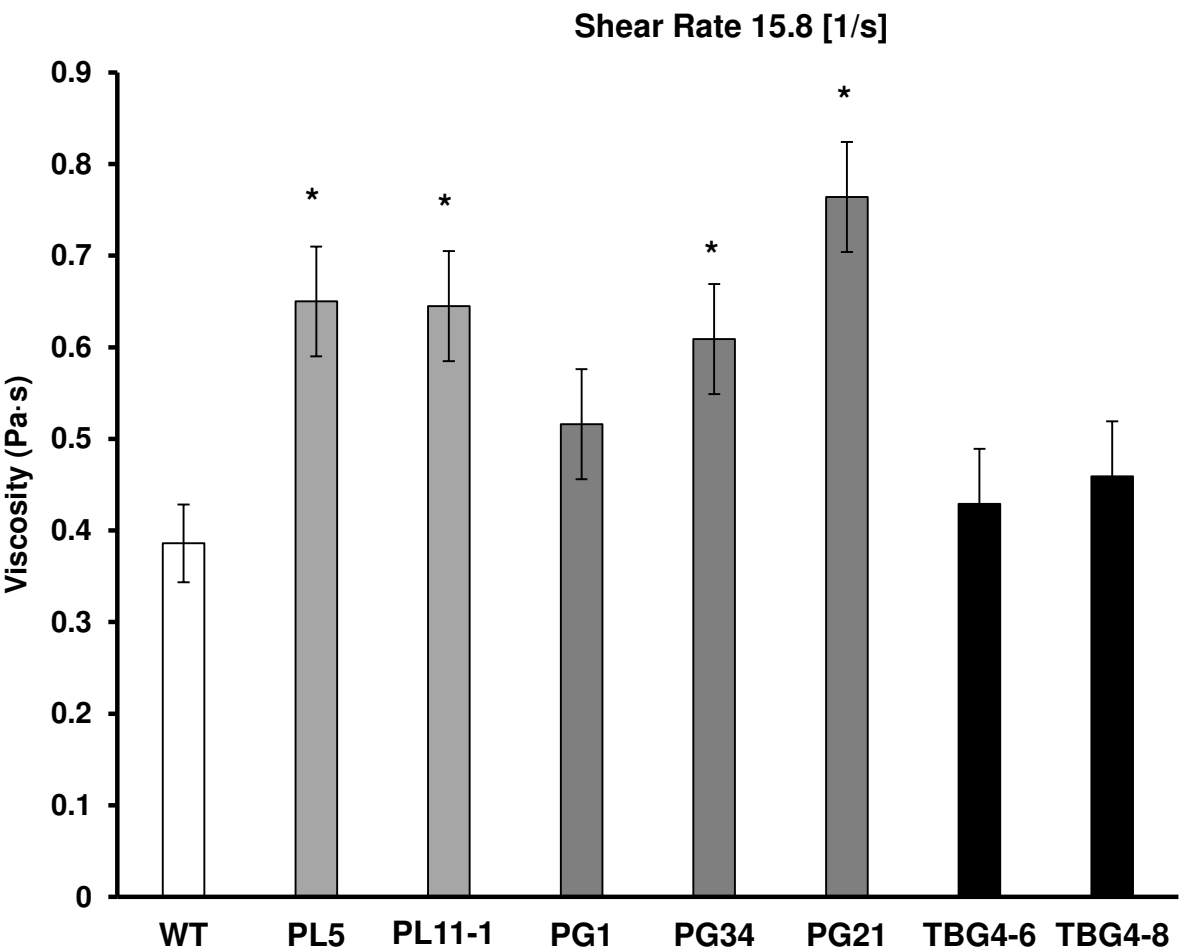

Figure 6. Transmission electron micrographs of cell junctions from the pericarp of the CRISPR lines. Sections cut from three separate fruits from each of wild type, *PL5*, *PG34* and *TBG-8* lines were visualised under the transmission electron microscope and two representative micrographs shown for each line. The scale bar on each micrograph represents 10 µm. TCI = tricellular junction and PCW = primary cell wall.

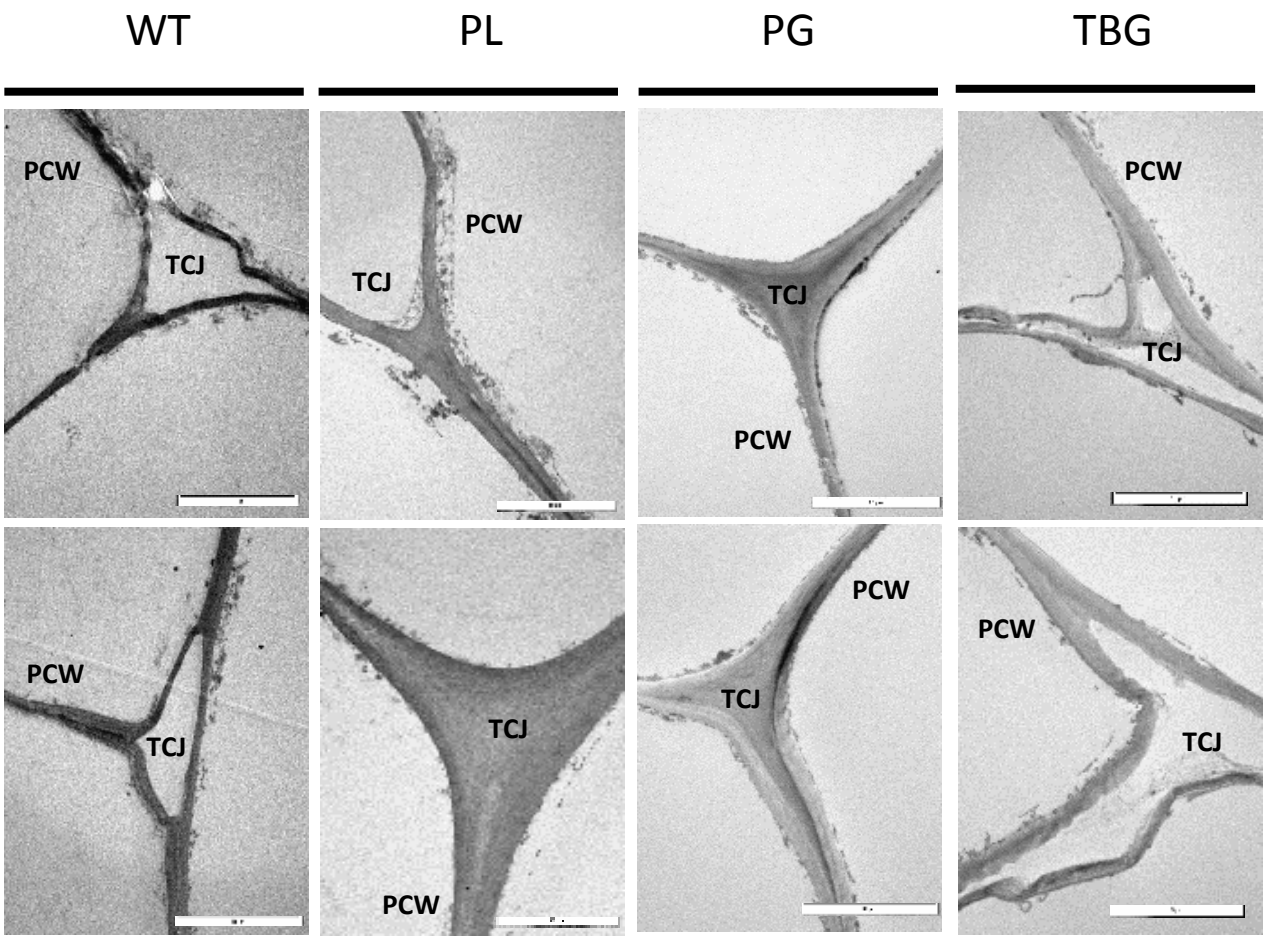

Figure 7. Immunolocalisation of deesterified pectin and pectic galactan in CRISPR lines. Monoclonal antibody probes recognising deesterified pectin (LM19) and pectin associated β-galactan (LM5) were used to label tomato pericarp tissue. For each probe low (A and C) and high magnification (B and D) images are presented. Representative sections of fruits from each of wild type, *PL5*, *PG34* and *TBG-8* lines are shown. Scale bar represents 100 µm at low magnification and 10 µm at high magnification. TCJ = tricellular junction, ML = middle lamella.

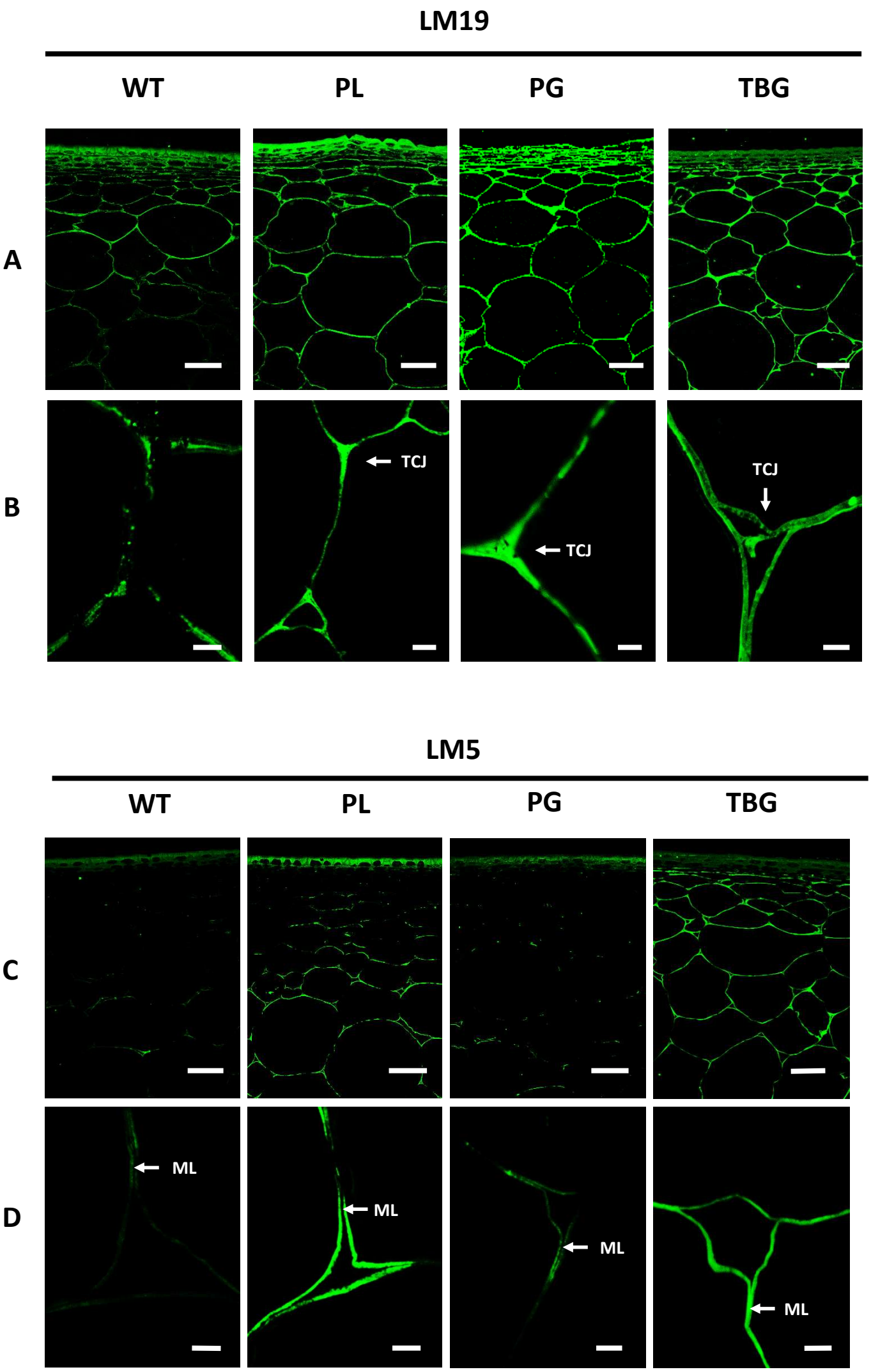

Figure. 8. Extraction and characterisation of cell wall pectin fractions using pectin antibody probes. Tomato cell wall materials from three biological replicates of breaker+7 fruit pericarp of wild type (WT), *PL*, *PG2a* and *TBG4* were fractionated/sequentially solubilized with water, cyclohexane diamine tetraacetic acid (CDTA), 4 M potassium hydroxide and by treatment with cellulase. The resulting sequential extracts were serially diluted and analysed with monoclonal antibodies and data for 6250x dilutions are shown. Antibodies used were (A) LM19 to un-esterified homogalacturonan, (B) LM5 to (1-4)-β-galactan, (C) INRA-RU1- to the RG-I backbone and (D) LM6 to (1-5)-α-arabinan. Levels of specific pectic polysaccharide epitopes were detected as detailed in the materials and methods. Data were analysed a Duncan's Multiple Range Test. Where significant ($P<0.05$) differences occur between tomato genotypes with the same extractant these are shown by different letters.

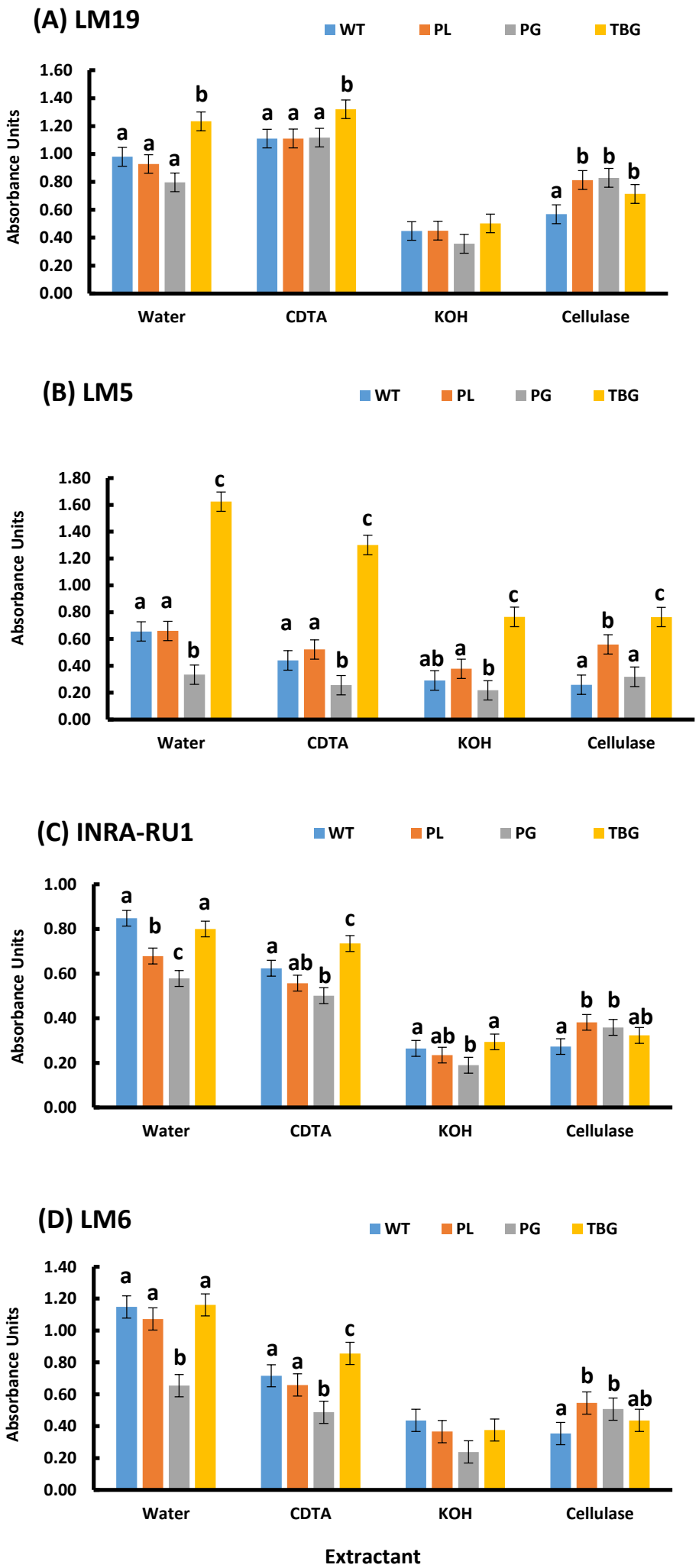

Table S1. Target sequences of cell wall structure-related genes

Target Gene	Gene identifier	Gene Product	Target site (5'-3′) (PAM is underlined)
PL	Solyc03g111690	Pectate lyase	GGGCGCTAGCGTACACATAGCGGG
PG-2a	Solyc10g080210	Polygalacturonase	GTGATTAATGTACTTAGCTTTGG
TBG4	Solyc12g008840	Beta-galactosidase	GGCCATACAATCTGCCTCCATGG

Table S2. Fresh weight / dry weight ratios of pericarp sections from three independent wild type (WT) and *PG2a*, *PL* and *TBG4* lines. The overall variation among the means was not significant (F3,8df=2.76; P=0.111).

Sample	**Fresh weight / dry weight**
Wild type	15.03 ± 1.08
PG2a	17.03 ± 1.08
PL	19.37 ± 1.08
TBG4	17.78 ± 1.08

Table S3. Fluorescence intensity based on analysis of sections in the confocal microscope at 10x objective with ImageJ and using Duncan's Multiple Range Test to compare lines. Values in body of table are mean intensity for each antibody probe, LM19 or LM5 ± SEM, n=3.

Probe	Wild type	PL	PG2a	TBG4
LM19	61.7 ± 9.42 a	96.2 ± 9.42 b	103.2 ± 9.24 b	84.4 ± 9.42 ab
LM5	34.5 ± 8.15 a	114.2 ± 8.15 b	38.9 ± 8.15 a	115.2 ± 8.15 b

Table S4. Primer sequences for amplifying sgRNAs

Name	Sequence
PL-sgRNA-F	TGTGGTCTCAATT**GGGCGCTAGCGTACACATAGC**GTTTTAGAGCTAGAAATAGCAAG
PG2a-sgRNA-F	TGTGGTCTCAATT**GTGATTAATGTACTTAGCTT**GTTTTAGAGCTAGAAATAGCAAG
TGB4-sgRNA-F	TGTGGTCTCAATT**GGCCATACAATCTGCCTCCA**GTTTTAGAGCTAGAAATAGCAAG
sgRNA-R	TGTGGTCTCAAGCGTAATGCCAACTTTGTAC

Table S5. Primer sequences for genotyping of CRISPR/Cas9-induced mutations

Purpose	Primer Name	Primer Sequence (5'-3')
Verification of CRISPR/Cas9 transgene	pAGM4723 F3	CCTGTTTGGTAATCTTATCGC
	pAGM4723 R3	CCTCTTCAATCCTCTTCATCC
Genotyping *PL*	PL-RE-F	GTGGTACCGGAAATCCAATC
	PL-RE-R	CAATGATCCACCCAAACATG
Genotyping *PG2a*	PG-RE-F	CAAAGGAATAGTATTCTCCTTCTC
	PG-RE-R	CAGTTCCATGGAAAATGACTTTC
Genotyping *TBG4*	TBG-RE-F	TCCAGATCCCACTATGTGAGACTAC
	TBG-RE-R	CTATACCTGTGCAGTGTTGTAAACG

Table S6. Primer sequences for qPCR relative expression analyses

Primer Name	**Primer Sequence (5'-3')**
PL-RT-F	GAATGCCAAGATGTAGACATGG
PL-RT-R	CCTCTTTGCTAAACCTGATATCAG
PG2A-RT-F	AAGACTTGGCAGGGAGGATC
PG2A-RT-R	TATGGCCACCTTTGTTGCAC
TBG-RT-F	GTCAATGGAAAACTATCAGGAACTG
TBG-RT-R	CTGCATTCCATGTATCATAATGCAC
Solyc05g055510-F	AGGTGATGGAATTAGCAACCA
Solyc05g055510-R	GAAATGCAGATTTAGGCTCCA
Solyc02g093580-F	AAGACGTTCATAGGAGCATCAAT
Solyc02g093580-R	GATCCGCACGATAAATAGCC
Solyc06g083580-F	CACGCACTGGGAGATGTATG
Solyc06g083580-R	CCCTGGCTGTTAATTGTAGGA
Solyc08g060970-F	TGTCCGAGTCCAGTTCCTGT
Solyc08g060970-R	TCCATCTCCAAAAGCGCCAT
EF-1a-F	GACAAGAAGGACCCAACTGGTG
EF-1a-R	CAGAGTCTAGATAGCACACTCGATG

Figure S1. Amino acid sequence analysis of PL in wild type and CRISPR lines. Sequence in pink represents the polypeptide in the wild-type (WT) protein. The sequence highlighted in grey refers to an alteration in the encoded amino acid sequence in the CRISPR lines *PL5* or *PL11-1* which introduces a stop codon.

WT

Met G T S S V F L L F L L S F L L L L P S L L A S S N P Q Q V V
D E V H R S I N G S R R N L G Y L S C G T G N P I D D C W R C D
P N W E K N R Q R L A D C A I G F G K N A I G G R D G K I Y V V
T D S G D D N A V T P K P G T L R H A V I Q T E P L W I I F A R
D M V I Q L K E E L I M N S F K T I D G R G A S V H I A G G P C
I T I Q Y V T N I I I H G I H I H D C K Q G G N A M V R S S P S
H Y G W R T V S D G D G V S I F G G S H V W V D H C S L S N C K
D G L I D A I Met G S T A I T I S N N Y M T H H D K V M L L G H
S D T Y T Q D K N M Q V T I A F N H F G E G L V Q R M P R C R H
G Y F H V V N N D Y T H W E M Y A I G G S A D P T I N S Q G N R
F L A P D I R F S K E V T K H E D A P E S E W K N W N W R T D G
D L M L N G A F F T R S G V R T G S S S Y A K A S S L S A R P S
S L V A N L V S S S G A L N C K K G S R C Stop

PL5

Met G T S S V F L L F L L S F L L L L P S L L A S S N P Q Q V V
D E V H R S I N G S R R N L G Y L S C G T G N P I D D C W R C D
P N W E K N R Q R L A D C A I G F G K N A I G G R D G K I Y V V
T D S G D D N A V T P K P G T L R H A V I Q T E P L W I I F A R
D M V I Q L K E E L I M N S F K T I D G R G A S V H I S G W S V
Y N N T V R N E Y Y Y T R N S Y T Stop

PL11-1

Met G T S S V F L L F L L S F L L L L P S L L A S S N P Q Q V V
D E V H R S I N G S R R N L G Y L S C G T G N P I D D C W R C D
P N W E K N R Q R L A D C A I G F G K N A I G G R D G K I Y V V
T D S G D D N A V T P K P G T L R H A V I Q T E P L W I I F A R
D M V I Q L K E E L I M N S F K T I D G R G A S V H M S G W S V
Y N N T V R N E Y Y Y T R N S Y T Stop

Figure S2. Amino acid sequence analysis of *PG2a* in wild type and CRISPR lines. Sequence in pink represents the polypeptide in the wild-type (WT) protein. The sequence highlighted in grey refers to an alteration in the encoded amino acid sequence in the CRISPR lines *PG34*, *PG21* or *PG1* which introduces a stop codon.

WT

Met V I Q R N S I L L L I I I F A S S I S T C R S N V I D D N L
F K Q V Y D N I L E Q E F A H D F Q A Y L S Y L S K N I E S N N
N I D K V D K N G I K V I N V L S F G A K G D G K T Y D N I A F
E Q A W N E A C S S R T P V Q F V V P K N K N Y L L K Q I T F S
G P C R S S I S V K I F G S L E A S S K I S D Y K D R R L W I A
F D S V Q N L V V G G G G T I N G N G Q V W W P S S C K I N K S
L P C R D A P T A L T F W N C K N L K V N N L K S K N A Q Q I H
I K F E S C T N V V A S N L M I N A S A K S P N T D G V H V S N
T Q Y I Q I S D T I I G T G D D C I S I V S G S Q N V Q A T N I
T C G P G H G I S I G S L G S G N S E A Y V S N V T V N E A K I
I G A E N G V R I K T W Q G G S G Q A S N I K F L N V E M Q D V
K Y P I I I D Q N Y C D R V E P C I Q Q F S A V Q V K N V V Y E
N I K G T S A T K V A I K F D C S T N F P C E G I I M E N I N L
V G E S G K P S E A T C K N V H F N N A E H V T P H C T S L E I
S E D E A L L Y N Y Stop

PG34

Met V I Q R N S I L L L I I I F A S S I S T C R S N V I D D N L
F K Q V Y D N I L E Q E F A H D F Q A Y L S Y L S K N I E S N N
N I D K V D K N G I K V I N V L T L E L R VMet E K H Met I I L
H L S K H G Met K H V H L E H L F N L W F L K T R I I F S S K S
P F Q V H A D L L F Q Stop

PG21

Met V I Q R N S I L L L I I I F A S S I S T C R S N V I D D N L
F K Q V Y D N I L E Q E F A H D F Q A Y L S Y L S K N I E S N N
N I D K V D K N G I K V I N V L S L W S Stop

PG1

Met V I Q R N S I L L L I I I F A S S I S T C R S N V I D D N L
F K Q V Y D N I L E Q E F A H D F Q A Y L S Y L S K N I E S N N
N I D K V D K N G I K V I N V P L E L R V M E K H Met I I L H L
S K H G M K H V H L E H L F N L W F L K T R I I F S S K S P F Q
V H A D L L F Q Stop

Figure S3. Amino acid sequence analysis of *TBG4* in wild type and CRISPR lines. Sequence in pink represents the polypeptide in the wild-type (WT) protein. The sequence highlighted in grey refers to an alteration in the encoded amino acid sequence in the CRISPR lines TBG4-6 and TBG4-8 which introduces a stop codon.

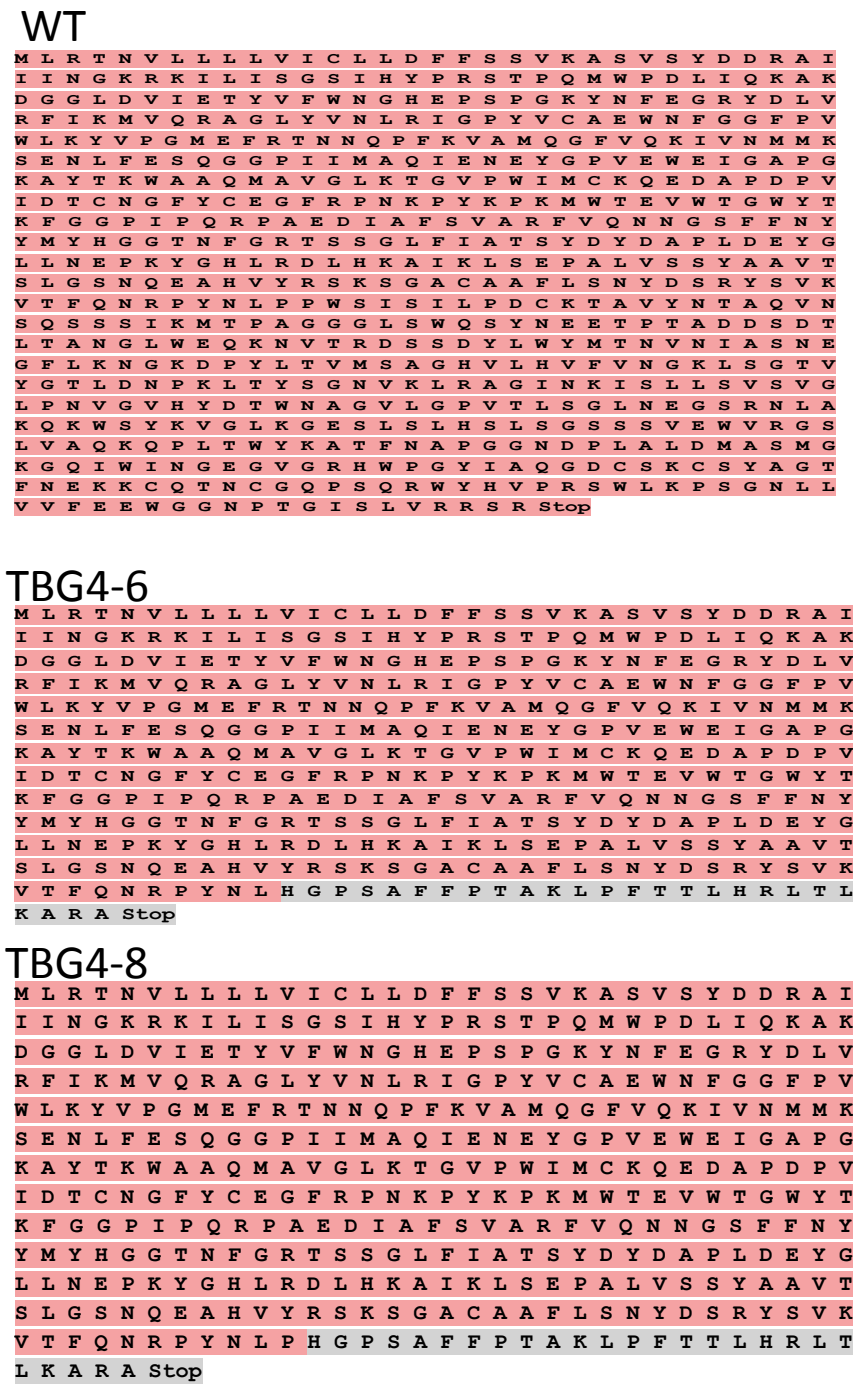

Figure S4. Relative expression of target genes in CRISPR mutants in *PL*, *PG2a* and *TBG4* lines. Target gene expression was measured in three fruit of each line at breaker +7 days. Error bars represent ± sem, n=3. Significant differences between mutants and wild type control based on a Dunnet's test were marked by *** P<0.001.

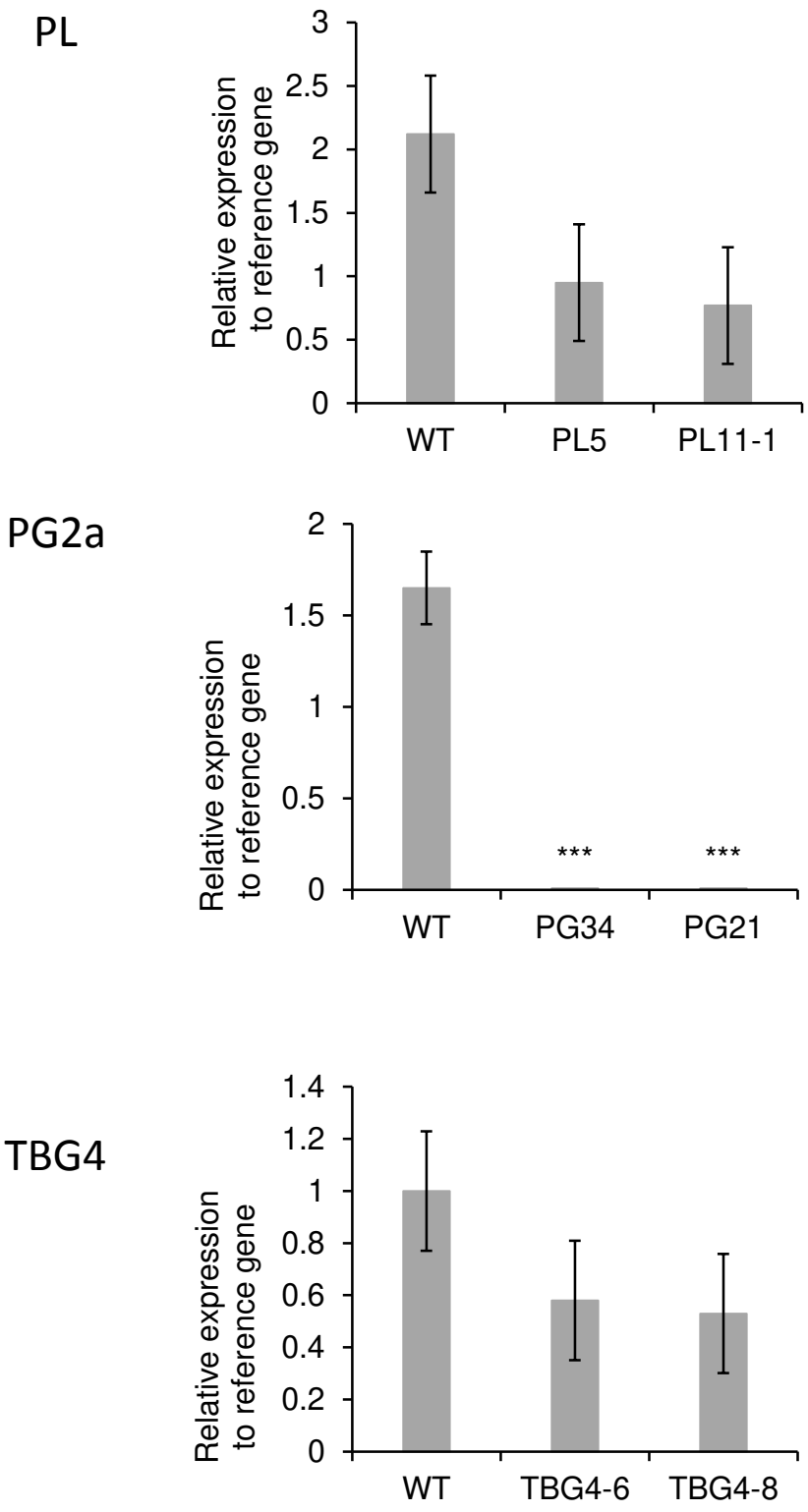

Figure S5. Expression of *PL* and *PG2a* gene family members in the CRISPR linesmat the Breaker + 7 stage. Error bars represent ± SEM, n=5. Significant differences determined by t-test comparisons with wild type are denoted by * (P<0.05 *), (P<0.01 **), (P<0.001 ***).

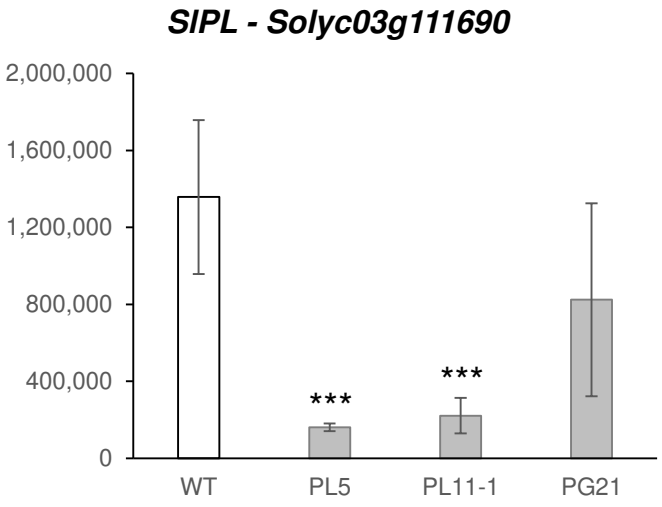

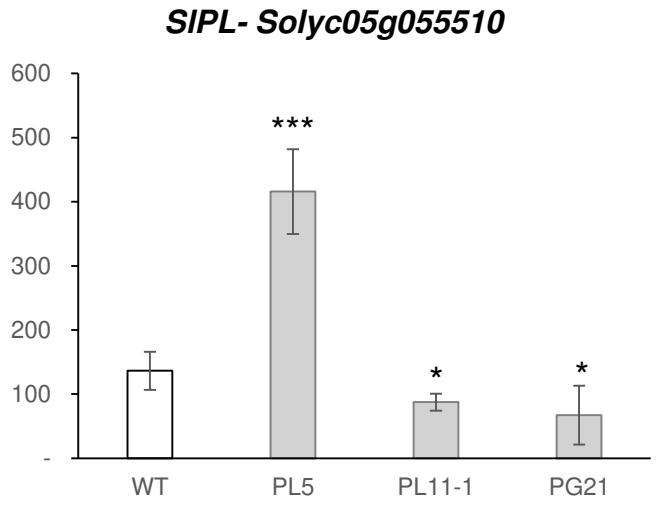

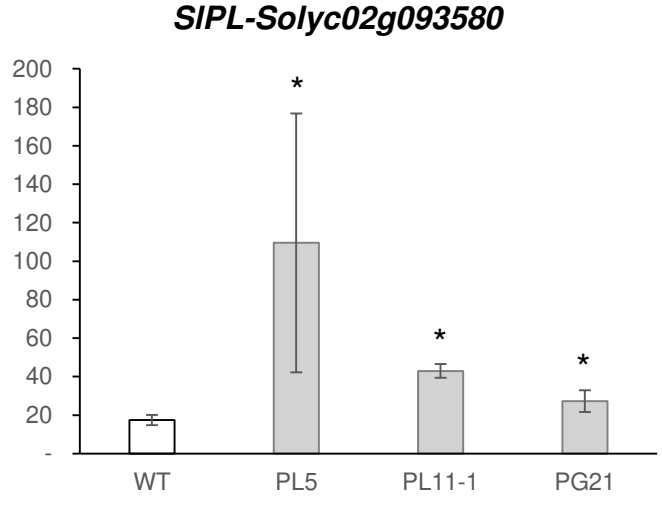

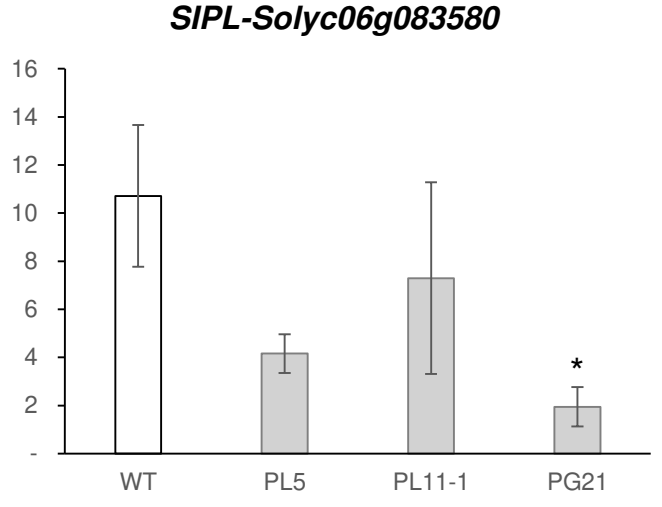

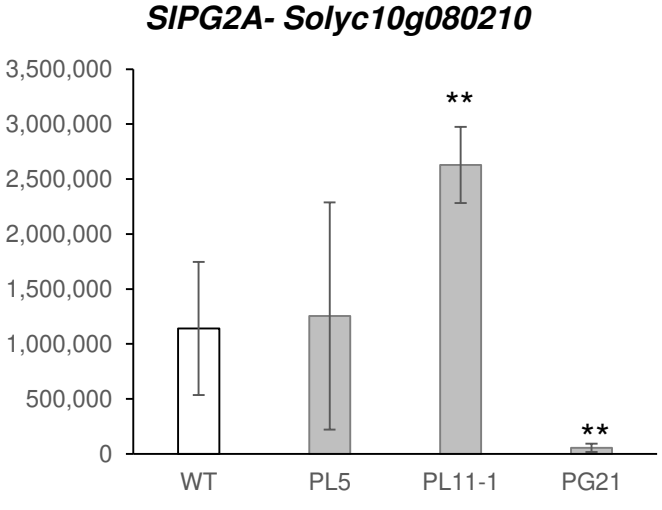

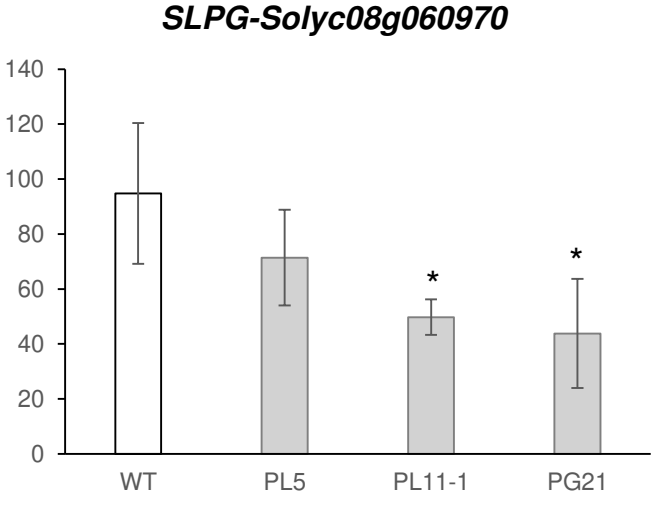

Figure S6. β-galactosidase activity in TBG4 CRISPR lines measured as specific activity / mg of protein

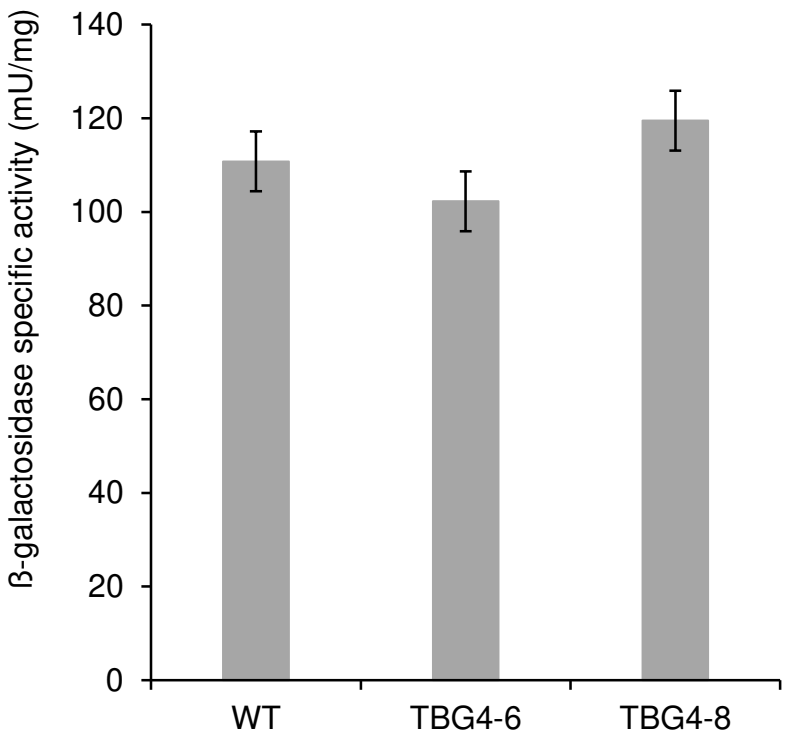

Figure S7. Carotenoid levels in the ripe fruits of the CRISPR lines. Carotenoids were extracted at Breaker +7 with three biological replicates for each line. The data were analysed to test for differences among lines using the Duncan's Multiple Range Test. Only changes in β-carotene and cis-phytoene were significant at ($P<0.05$) and are denoted by letters above the bars.

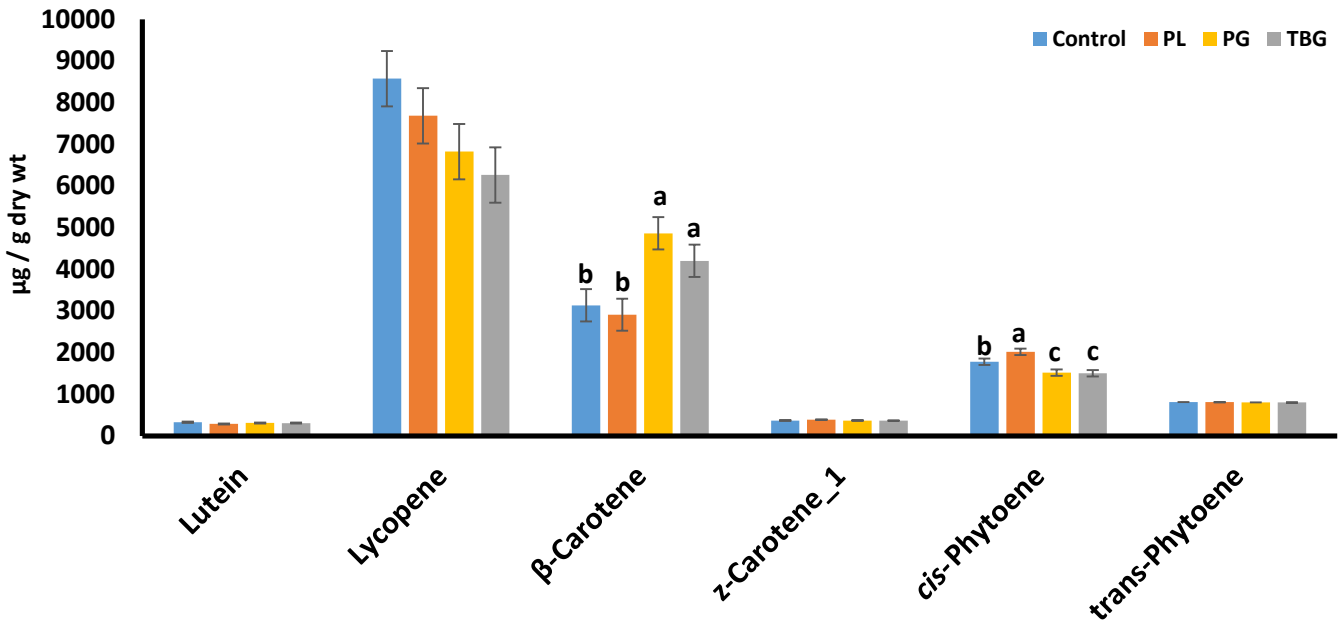

Figure S8. Calcofluor white staining of pericarp sections from CRISPR lines. Fruits from *PL5*, *PG34* and *TBG-8*. Sections show (A) outer and (B) inner pericarp. Scale bar = 100µm.